Equilibrium Molecular Dynamics Study of Heat Conduction in Octane

by

Yi Jenny Wang

Submitted to the Department of Mechanical Engineering
in partial fulfillment of the requirements for the degree of

Master of Science in Mechanical Engineering

at the

MASSACHUSETTS INSTITUTE OF TECHNOLOGY

February 2015

Signature redacted

Author . . . . . .
Department of Mechanical Engineering
January 29, 2015

Signature redacted

Certified by . . . . . .
Gang Chen
Carl Richard Soderberg Professor of Power Engineering
Thesis Supervisor

Signature redacted

Accepted by . . . . . .
David E. Hardt
Chairman, Department Committee on Graduate Students

Equilibrium Molecular Dynamics Study of Heat Conduction in Octane

by

Yi Jenny Wang

Submitted to the Department of Mechanical Engineering
on January 29, 2015, in partial fulfillment of the
requirements for the degree of
Master of Science in Mechanical Engineering

Abstract

Fluids are important components in heat transfer systems. Understanding heat conduction in liquids at the atomic level would allow better design of liquids with specific heat transfer properties. However, heat transfer in molecular chain liquids is a complex interplay between heat transfer within a molecule and between molecules. This thesis studies the contribution of each type of atomic interaction to the bulk heat transfer in liquid octane to further the understanding of thermal transport between and within chain molecules in a liquid. The Green-Kubo formula is used to calculate thermal conductivity of liquid octane from equilibrium molecular dynamics, and the total thermal conductivity is split into effective thermal conductivities for the different types of atomic interactions in the system. It is shown that the short carbon backbone of octane does not dominate thermal transport within the system. Instead, the thermal resistance within a molecule is about the same as the resistance between molecules.

Thesis Supervisor: Gang Chen
Title: Carl Richard Soderberg Professor of Power Engineering

Acknowledgments

I would like to thank my adviser Professor Gang Chen for his advice and support. I also thank former lab mates Tengfei Luo, now assistant professor at the University of Notre Dame, for teaching me the basics of molecular dynamics, and Zhiting Tian, now assistant professor at Virgina Tech for further guidance and help with the simulations. Additional thanks go to everyone in the NanoEngineering group for the insights, discussions, and companionship over the last few years. Outside of lab, I am grateful for my parents. I would not be the person I am today without their love, support, and guidance. I would also like to thank all my friends at Sidney Pacific; life at MIT would not be the same without all of them.

Contents

List of Figures

List of Tables

Chapter 1

Introduction

Understanding thermal conductivity of fluids at the atomic level would provide the necessary insights to improve heat transfer in fluids. Fluids play vital roles in heat transfer systems as heat exchange mediums. These applications use the bulk heat transfer properties of the fluid. However, an atomic level understanding of heat conduction in fluids can enable us to design fluids with specific thermal properties, and make it possible to exploit specific atomic-level properties to design materials that may become critical components of the future's ever smaller electronic devices. Understanding heat transfer in chain liquids at an atomic level is difficult because there are two distinct contributions to transport. In this thesis, chain liquids refers to liquids that are made up of chain molecules. On one hand, long molecular chains can effectively transport heat along the chain backbone [1], which is similar to phonon transport in solids [2]. On the other hand, the chains are also free to flow from one area of the system to another, which is similar to transport in gases and can be described by kinetic theory and statistical mechanics [3]. Additionally, any heat transfer pathway through the liquid system involves heat transfer both within a molecule (intramolecular heat transfer) and between molecules (intermolecular heat transfer), as

demonstrated in figure 1-1. Understanding this interplay is at the heart of understanding bulk heat transfer in liquids with molecular chains.

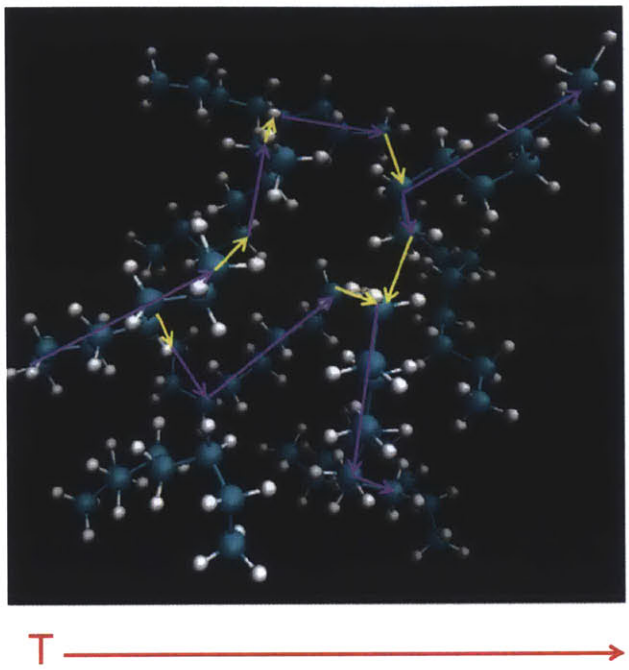

Figure 1-1: In a system like bulk octane, there are multiple pathways for heat to flow from the hot side of the system to the cold side (the red arrow marks the temperature gradient from high to low). Some possible pathways are marked in the diagram as examples. Any heat pathway, however, involves both intramolecular (purple) and intermolecular (yellow) paths. Thus, both atomic interactions within an octane molecule and interactions between separate molecules play important roles in heat transport of bulk octane.

All heat transfer, at the atomic level, is energy transfer through atomic interactions. Interactions between atoms connected by covalent or ionic chemical bonds can be collectively called "bonded interactions" while interactions between atoms not chemically bonded together (i.e. on different molecules) are referred to as "non-bonded interactions." Non-bonded interactions include electrostatic forces and van der Waals forces. The interactions in the octane system will be further described in chapter 2.

The liquid system studied in this work is octane. Octane is a chain of eight carbon atoms single bonded to each other with 18 hydrogens on each molecule to fill out the carbon orbitals. An artistic rendering of the octane molecule is shown in figure 1-2. The choice of using octane was influenced by several factors. First, as a simple organic molecule, the interactions between the atoms within the system is well understood. Molecular biology has developed many potentials to accurately reproduce different aspects of organic chemistry interactions [4]. In contrast, many elements that are not commonly encountered in organic chemistry have not been as well studied. Second, the alkane series is the simplest organic chain molecule. The simplicity of the system is important because it allows a starting point to study the complicated interplay of heat transfer at the atomic level. Third, because octane is the primary component in gasoline, the literature on octane is much more extensive than other alkanes of similar lengths. For example, a search on Web of Science [5] in January 2015 yielded 6167 articles with "octane" in the title versus 1778 articles with "nonane" in the title. The available literature serves as important grounding points for the calculations. The molecular dynamics (MD) simulations were performed using the Large-scale Atomic/Molecular Massively Parallel Simulator (LAMMPS) [6, 7] developed at Sandia National Laboratories.

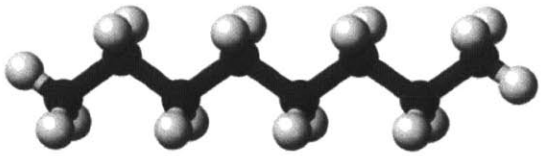

Figure 1-2: Rendering of an octane molecule. Carbon atoms are black while the hydrogen atoms are white.

1.1 Heat Transfer in Lennard-Jones Fluids

Recently, it has become possible to directly study atomic level heat transfer in solids experimentally [8], and there are a number of experiments measuring thermal transport in interfaces and atomic junctions [9, 10, 11, 12]. Modeling, however, remains an important aspect of understanding the atomic level processes in liquids. At the simplest level, heat transfer in liquids can be modeled using a Lennard-Jones potential [13, 14]. First proposed by John Edward Lennard-Jones in 1924 [15], the Lennard-Jones potential describes a simple potential well between two particles and is often written as

$$V_{LJ} = 4\epsilon \left[\left(\frac{\sigma}{r}\right)^{12} - \left(\frac{\sigma}{r}\right)^{6} \right] \tag{1.1}$$

where ϵ is the depth of the potential well, σ is the finite distance when V_{LJ} is zero, and r is the distance between the two particles. The values of ϵ and σ can be fitted to experimental values to adapt the potential to a range of different atoms and small molecules. However, if the potential is expressed in terms of $\frac{V_{LJ}}{\epsilon}$ and $\frac{\sigma}{r}$, then there are no additional terms in equation (1.1), and it becomes apparent that there is only one Lennard-Jones potential (figure 1-3). Indeed, the term Lennard-Jonesium is often used to refer to the theoretical fluid that is perfectly described by the Lennard-Jones potential [16]. In reality, there is no true Lennard-Jones material of course, but the approximation is fairly good for certain molecules with simple atomic interactions, such as the nobel gases [17, 18], with argon being especially popular for study. The thermal conductivities of liquid argon have been calculated from Lennard-Jones potentials using MD with error less than 10% when compared to experiments [14].

There are two ways to calculate thermal conductivity using MD: the equilibrium and non-equilibrium approach. The equilibrium approach, which is the method used in this thesis, relies on the Green-Kubo formula to connect local fluctuations in heat

flux to the thermal conductivity [19]. More details are given in chapter 3. The non-equilibrium approach imposes a heat flux or temperature difference on the system and determines the thermal conductivity by fitting the data to Fourier's Law

$$q = -\kappa \frac{dT}{dx} \tag{1.2}$$

where q is the heat flux, κ is the thermal conductivity, and $\frac{dT}{dx}$ is the spatial temperature gradient in the system [20, 21].

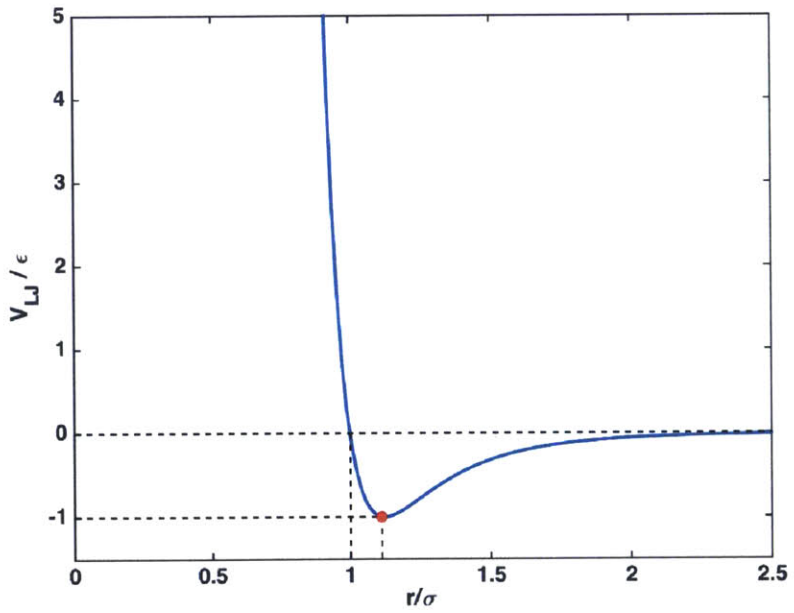

Figure 1-3: The Lennard-Jones potential normalized by ϵ and σ, where ϵ is the depth of the potential well and σ is the finite distance where V_{LJ} is zero. When normalized this way, there is only one Lennard-Jones potential. The equilibrium distance between two atoms interacting according to the Lennard-Jones potential is the separation that gives the minimum energy and is marked with a red dot. As distances becomes much smaller than equilibrium, the potential increases towards infinity, representing the strong repulsion from electrons on each atom. As the separation distance approaches infinity, the potential goes to zero, representing the weakening interaction as the two atoms become further apart.

Before the advent of computers powerful enough to run MD simulations, the Lennard-

Jones potential was already being used in statistical mechanics to aid understanding of thermal transport in fluids. A great deal of the statistical mechanics theory was developed in the 1950s [22, 23], including the Green-Kubo relations [24, 25] used in this work. Details of the the Green-Kubo relation for thermal conductivities are in chapter 3. From the hydrodynamic equation in statistical mechanics, the thermal conductivity of argon modeled using the Lennard-Jones potential has been calculated to be $\kappa = 0.17$ W/(m K) [23], which compares well with the experimental value of $\kappa = 0.12$ W/(m K) [26]. Furthermore, the kinetic energy contribution (contribution from motion of argon atoms) to thermal conductivity is negligible and heat is primarily transferred through the intermolecular force (interactions between argon atoms) contribution [23]. Molecular dynamics studies confirm that the kinetic energy contribution is only a few percent of the total heat transfer [14]. However, this may be because the boiling point of argon is low, around 87 K. In liquids at room temperature, the kinetic energy play a more significant role [27]. For liquid argon, contribution of kinetic energy to heat transfer depends heavily on system density, increasing by more than a factor of 2 when the density changes by 20% while the intermolecular force contribution has little to no dependence on density [14]. Results for Lennard-Jones liquids using equilibrium MD and non-equilibrium MD compare fairly well, and both are consistent with experimental values. In equilibrium MD, the thermal conductivity of Lennard-Jones liquid has little dependence on the system size with good convergence for systems containing as few as 108 atoms [14]. In contrast, non-equilibirum MD requires a bigger system to reach a good convergence [28]. The accuracy of the small system in equilibrium MD may be because intermolecular heat transfer between first neighbors dominate thermal transport in this system [29] so additional neighbors are not as important. The temperature gradient or heat flux must be imposed on the system in non-equilibrium MD so the system must be large enough to support the required difference from one side to the other.

1.2 Effect of Atomic Structure

While sufficient for simple materials like argon, the basic Lennard-Jones potential can only describe one type of atomic interaction, is limited to pairs interactions (interactions involving only two atoms) and models molecules as spheres so it cannot describe the structure of multi-atom molecules. The two-center Lennard-Jones potential [30] adds rotational degrees of freedom to the system and accounts for atomic separation in a molecule to allow more accurate modeling of diatomic molecules. The two-center Lennard-Jones potential is a sum of the basic Lennard-Jones potential adapted to molecules having two centers. For two molecules, i and j, the two-center Lennard-Jones potential is

$$V_{2cLJ} = \sum_{a=1}^{2} \sum_{b=1}^{2} V_{LJ}\left(r_{ia,jb}\right) \tag{1.3}$$

where $r_{ia,jb}$ is the separation between centers a on molecule i and b on molecule j and V_{LJ} is the basic Lennard-Jones potential in equation (1.1). This type of potential allows investigations on the dependence of thermal conductivity on molecule length in diatomic molecules and the role of rotational degrees of freedom. As separation between the atoms in a diatomic molecule become longer, non-equilbrium molecular dynamics shows that the thermal conductivity increases slightly, primarily due to increased heat transfer in intermolecular interactions from rotational degrees of freedom, and heat transfer due to molecular motion is not affected [31]. Heat transfer due to molecular motion is also not affected significantly by increases in liquid density or pressure. Instead, the thermal conductivity increase in these situations are due to increased heat transfer by molecular interactions [32].

More complicated molecules contain atoms and bonds with very different characteristics and require more complex potentials to fully describe the atomic interactions present in the system. Many potentials have been developed to describe different types

of systems over the year. Commonly used classical potentials include the Optimized Potentials for Liquid Simulations (OPLS) [33], Chemistry at HARvard Molecular Mechanics (CHARMM) [34], Assisted Model Building and Energy Refinement (AMBER) [35], GROningen MOlecular Simulation (GROMOS) [36] among others. These classical potentials typically all have similar forms of the interactions but have parameter values fitted to very different physical properties. This work uses the GROMOS potential, which is fitted to free enthalpy and energy of solvation. Further details of the GROMOS potential are presented in section 2.2. Many studies using the various classical potentials have produced thermal conductivities comparable to experimental values, establishing the basic methods of calculating thermal conductivity in MD [37, 38, 39, 40, 27, 41, 42, 43]. These simulations show that the conformation of molecules play significant roles in liquid thermal conductivity [40] but conformation is often dependent on the potential used since each potential has different interaction parameters and forms. Additionally, equilibrium and non-equilibrium MD can yield different results for thermal conductivity since these methods make different assumptions about the system. Thus, having data from both methods is valuable to verify results.

1.3 Heat Transfer in Carbon Chains

Degrees of freedom within the molecule adds significant complexity to the atomic heat transfer picture. Unlike Lennard-Jones liquids, where interactions are fairly isotropic, the interatomic forces in alkanes are very anisotropic due to the large difference in strength between bonded interactions along the chain and non-bonded interactions across the chain. The thermal conductivity of stretched polyethylene fibers have been measured to be over 100 W/(m K) [44]. In comparison, thermal conductivity of bulk polyethylene is around 0.3 W/(m K). Simulations show that the drastic in-

crease in thermal conductivity can be explained by the high thermal conductivity of the carbon-carbon backbone [1] and the stretching process extending and aligning the polyethylene molecules to better take advantage of heat transfer along the backbone [45, 46]. Restricting the rotation of C-H_2 segments within the molecule further increases thermal conductivity [47]. Thermal conductivity of polymers depends on the molecule length as well, with longer molecules being more conductive [1, 48, 49]. More rigid backbones and stronger intermolecular interactions also increases thermal conductivity [50, 51]. All these strategies for increasing heat transfer in polymers are essentially increasing phonon transport within the polymer by making the structure more crystalline and strengthening the atomic interactions.

Liquids, by definition, cannot be made crystalline, and allowing molecules to flow from one part of the system to another further complicates the heat transfer picture. However, the smaller molecules of liquid alkanes (in comparison to polymers) allow more detailed analysis of the specific types of atomic interactions, which are not considered in the phonon picture. Non-equilibrium MD studies on alkane have split the total heat flux into contributions from each type of atomic interaction, including molecular motion, intermolecular interactions, bond stretching, and bond bending [27, 52]. However, these works used the united-atom approach which treats each C-H_2 segment in the alkane molecule as a single particle rather than explicitly accounting for the hydrogen atoms. Nevertheless, they offer important insights into heat transport in liquid carbon chains. In these liquid systems, molecular motion contributions toward heat transfer is dramatically higher than in liquid argon, accounting for around 20% of the total heat transfer. Furthermore, as the carbon chain becomes longer, intramolecular heat transfer becomes more important (table 1.1). In short alkanes, intramolecular interactions carry more heat than intermolecular interactions while the reverse is true for long alkanes. The cross-over occurs somewhere between chains containing 10 and 16 carbon atoms [27]. As the chain becomes even longer, intramolecular interactions account for even more of the total heat flux, increasing to

over 50% in alkanes with 24 carbon atoms. In contrast, heat transfer by molecular motion decreases only slightly as the alkane becomes longer.

Table 1.1: Percentage of the total heat flux due to intermolecular interactions, intramolecular interactions, and molecular motion in alkanes with different carbon chain lengths. Values are taken from [27].

Alkane	Intermolecular interaction	Intramolecular interaction	Molecular motion
C_4H_{10}	62%	13%	25%
C_8H_{18}	47%	30%	23%
$C_{10}H_{12}$	43%	33%	24%
$C_{16}H_{34}$	34%	43%	23%
$C_{24}H_{50}$	28%	53%	19%

This work aims to further the understanding of atomic level heat transfer in alkanes by providing equilibrium MD results for octane. The model used for octane here treats the hydrogen atoms explicitly and contains the slight differences in interaction for carbon and hydrogen atoms at different positions in the molecule. Thus, this model is more complete than those used in previous works. Chapter 2 covers the basics of understanding MD simulations. Next, the analysis tools used to understand heat transfer in the simulations, including a method of attributing fractions of the total thermal conductivity to each type of atomic interactions, are described in chapter 3. Chapter 4 contains the parameters used for the simulations in this thesis. Results from the analysis and discussions are presented in chapter 5. Finally, chapter 6 summarizes this thesis and gives some ideas for further exploration.

Chapter 2

Molecular Dynamics

Molecular dynamics (MD) is a numerical method to calculate atomic motion, which can give insights into fundamental properties of a system. As such, it is very widely used in materials and biological applications and have been applied to a wide range of phenomenons including diffusion, protein folding, defect formation, and heat transfer. This work uses MD as a tool to investigate atomic level thermal transport. This chapter will cover the basic knowledge required to understand MD simulations.

2.1 Basic Theory

Molecular dynamics simulation is essentially the application of Newton's second law, $\mathbf{F} = m\mathbf{a}$, to a system of particles in a series of time steps. The simplest MD codes require just three pieces of information about the system: 1) initial position of the particles, 2) the initial velocities of the particles, and 3) how the particles interact with each other (i.e. what forces the particles exert on each other). From initial positions, the code calculates the forces exerted on each particle by the other particles in the system. Applying Newton's second law to the forces on each particle gives

the particle's acceleration $\mathbf{a}$ as $\mathbf{a} = \mathbf{F}/m$. The initial velocity of each particle can then be used to calculate the particle's new position after a small time step dt by applying

$$\mathbf{r}_{t+dt} = \mathbf{r}_t + \mathbf{v}_t dt + \frac{1}{2}\mathbf{a}_t(dt)^2 \tag{2.1}$$

where $\mathbf{r}$ is the position and $\mathbf{v}$ is the velocity. The subscripts t and $t + dt$ denotes the value before and after the time step, respectively. The new velocity is

$$\mathbf{v}_{t+dt} = \mathbf{v}_t + \mathbf{a}dt \ . \tag{2.2}$$

The positions and velocities after the next time step is calculated using the updated positions and velocities, $\mathbf{r}_{t+dt}$ and $\mathbf{v}_{t+dt}$. The process is repeated until the required number of steps have been performed to give the total simulation time. Equations (2.1) and (2.2) are the Euler integration method, the simplest time-integration method for updating atomic positions and velocities from one time step to the next. In most time integration methods, the acceleration is constant during each time step. At small enough time steps, this is a satisfactory approximation. However, each time step uses values from the previous time step so errors accumulate and can be quite large by the end of the simulation. More sophisticated codes will calculate velocities and positions with different integration methods to minimize the error associated with the choice of dt. More details about the time integration used in this work is presented in section 2.3. The snap-shots of how the positions and velocities evolve over time are collectively called the atomic trajectory and are the raw data from the MD simulation. MD fundamentally requires the system to be ergodic [19]. That is, the time average is assumed to be the same as the phase space average so averages over the atomic trajectory can be used to obtain properties about the system. Figure 2-1 shows a summary of the MD simulation process.

Incredible achievements in computation speeds have been made since computers were first developed in the 1950s. However, computational power today still severely lim-

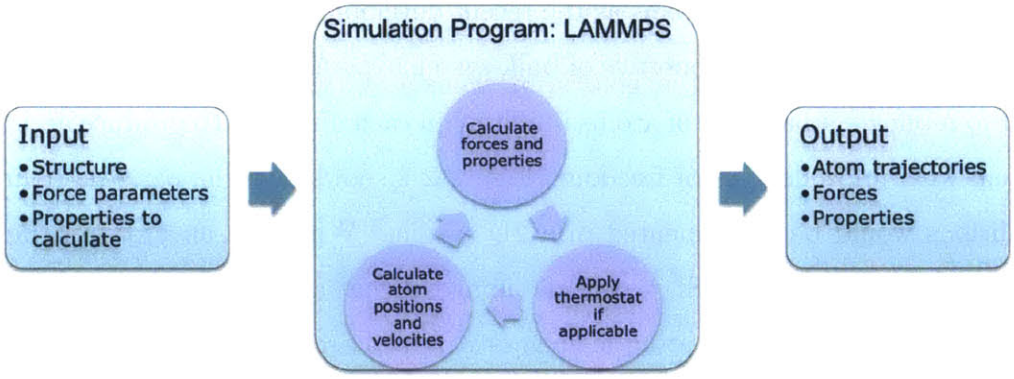

Figure 2-1: A summary of MD simulation using LAMMPS [6, 7]. Required inputs into the program are the atomic structure of the system, the force parameters describing atomic interactions, and the properties to be computed. For each time step, the LAMMPS program calculates the forces and requested properties, updates atomic positions and velocities, and adjusts system temperature, pressure, or volume as necessary. After the required number of time steps, the program produces the atomic trajectories, the forces within the system, and the averaged properties.

its the size of the molecular dynamics system that can be calculated in a reasonable time frame with reasonable computation resources. Calculating forces on each atom is a major part of the computation costs since this requires summing up the effect of the $N-1$ other atoms in the system on a particular atom. Typically, the number of required force calculations is reduced by recognizing that atomic interactions become negligibly weak at long enough distances so atoms that are further away than the cutoff distance are assumed to not interact directly. A major challenge to MD simulations are the different timescale at which the phenomenon to be studied occurs. The fastest motion in the system, typically the atomic vibrations, limit the maximum time step that can be used. A typical MD time step is around 1 fs and current computational capabilities limits the total number of time steps to $10^6 - 10^8$ so the total simulation time is limited to around 100 ns. Available computational capabilities also limit the maximum system size. Typical simulations can contain 10^4 to 10^8 particles, corresponding to a system size of 1 nm to 100 nm [53]. A system of this size, however, would have significant edge effects, and its properties would be

very different from bulk systems as the recent developments in nanotechnology make clear [54]. To reproduce properties of bulk systems, periodic boundary conditions are used to replicate a base cell of atoms infinitely in each direction to produce an infinite system with finite degrees of freedom. Figure 2-2 shows how the periodic boundary conditions would be implemented in a 2D system. Whenever an atom in the base cell moves outside of the cell, a periodic image of that atom enters the cell from the other side. Effectively, the atom leaving is wrapped around to the other side of the cell. The periodic boundary condition does not fully solve the edge effect error (for example, the longest phonon wavelength possible in a periodic system is twice the length of the periodic cell), but it eliminates surface forces (due to atoms at the edge of the system only having interactions on one side) and preserves the total energy of the system by preventing atoms from moving so far away that it no longer interacts with the rest of the system. The base cell size and the interaction cutoff radius must be chosen so that an atom cannot interact with multiple images of any other atom. This means that the base cell must be at least twice as wide as the cutoff radius, but is typically larger to ensure convergence with respect to system size.

2.2 Atomic Potentials

The methods used in MD intrinsically does not distinguish whether the particles represent atoms, molecules, or macro-level objects. Although the term "molecular dynamics" is typically reserved for molecular and atomic systems. Most MD programs only require the coordinates of initial particle locations and a set of interaction parameters describing the forces between the particles. The initial particle velocities are typically generated using a Gaussian distribution to match a desired temperature. For atomic or molecular systems, the required information is more naturally divided into a structure file that describes the initial locations of the atoms and the

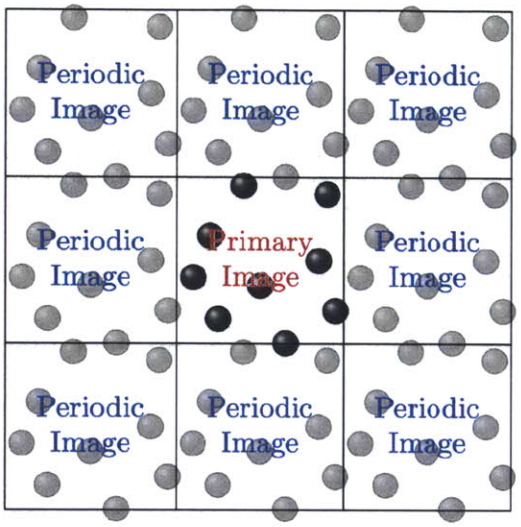

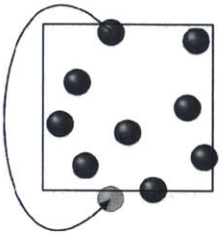

A particle leaving the primary image causes a periodic image to enter on the other side.

Figure 2-2: The periodic boundary condition applied in 2D. The base cell, which forms the primary image, is replicated in all directions to produce an infinite system. The effect is equivalent to having a particle that leaves the base cell enter on the opposite side. The base cell must be large enough so that no atoms interact with more than one image of any other atom.

chemical bonds within the system and a potential file that describes the force of each interaction type.

Using a suitable potential to describe the system is paramount to producing correct results. In contrast, slight errors in the initial positions of the atoms can be fixed by minimizing the total system energy with respect to an appropriate potential. Many potentials have been developed to suit the wide range of MD applications. Potentials are typically derived either using *ab initio* methods or fitted to some empirical parameters. Developing good potentials is a time consuming task that requires patience and experience. *Ab initio* potentials are generally more accurate than empirical potentials since they use quantum mechanics to calculate wave functions for the electrons in the system. The forces between the atoms are then calculated from the wave functions. However, this accuracy comes with very high computational costs when compared with empirical potentials. There are generally two components to

an empirical potential: 1) the mathematical functional form and 2) the parameters. The mathematical form is the expression that describes how the force acting on an atom depends on the atom's displacement from equilibrium while the parameters are constants within the form. Typically, the form is derived from some physical arguments and the parameters are selected to match a range of experimental or *ab initio* results. Therefore, each empirical potential is tailored for specific types of situations, but the commonly-used potentials generally apply to a wide range of systems and produce accurate results for a wide range of applications. By eliminating explicit calculations for elections, empirical potentials significantly improves the scaling of computations required for each additional atom in the system. Even larger systems can be accommodated by using coarse-graining methods, where a cluster of atoms are considered a single particle [55]. Then, potentials are developed to describe how each cluster particle interacts with other clusters in the system. A great deal of details are lost through coarse-graining but when investigating bulk behavior, the details are often not required. A common practice when modeling polymers is to coarse-grain the monomer so each unit in the polymer acts as a single entity. In this thesis, no coarse-graining is used and each atom in the system is treated explicitly.

The potential used in this work is GROningen MOlecular Simulation (GROMOS) 53A6 [36]. The potential was developed in conjunction with a molecular dynamics software also named GROMOS, but is widely supported in other MD programs. GROMOS started as a coarse-grain potential in the early 1980s by treating a carbon atom and attached hydrogen atoms as a single particle centered on the carbon atom. A substantial re-write occurred in 1996 to improve the treatment of aliphatic and aromatic hydrogens and the potential has been updated continuously since. While the parameters have been drastically improved over the years, the form of the potential has been preserved. GROMOS 53A6 still includes capabilities to treat carbon atoms and bonded hydrogen atoms as one particle, but it can also treat the carbon and hydrogen atoms as separate atoms. In this work, hydrogen and carbon atoms

are treated explicitly so each octane molecule contains 28 atoms. GROMOS 53A6 is designed to accurately reproduce the free energies in organic systems and have been used in biological applications with good results [56]. The GROMOS 53A6 functional forms and parameters used in this thesis are the stretching of covalent atomic bonds, bending of angles in covalent bonds, twisting of atomic dihedrals, a Lennard-Jones form for non-bonded interactions, and an electrostatic form for interactions between partial charges (see figure 2-3). This allows a detailed study of how each type of interaction contributes to the overall heat transfer. Although octane has no net charge, there are partial charges on some of the atoms since the electronegativity of carbon and hydrogen differs considerably. The forms and parameters given in GROMOS are for potential energies; the forces are calculated as the negative derivative of the energies with respect to the displacement: $\mathbf{F} = -\frac{\partial E}{\partial \mathbf{r}}$, where $\mathbf{F}$ is the force, E is the potential energy, and $\mathbf{r}$ is the displacement.

Potential energies due to covalent bonding is calculated by summing over all the bonds:

$$E_b^{GROMOS} = \sum_{n=1}^{N_b} \frac{1}{4} K_{bn}^{GROMOS} \left(b_n^2 - b_{0n}^2\right)^2 \tag{2.3}$$

where N_b is the total number of bonds, K_{bn}^{GROMOS} is the parameter describing the stiffness of the nth bond, b_n is the actual length of the nth bond, and b_{0n} is the equilibrium length of the nth bond. GROMOS developers chose this anharmonic functional form to reduce the number of square-root operations required to calculate forces, but, in the range of physically realistic values, it is essentially the same as the harmonic potential

$$E_b^{harmonic} = \sum_{n=1}^{N_b} K_{bn}^{harmonic} \left[b_n - b_{0n}\right]^2 \tag{2.4}$$

with $K_{bn}^{harmonic} = K_{bn}^{GROMOS} b_{n0}^2$ (see figure 2-4). The $E_b^{harmonic}$ functional form will be

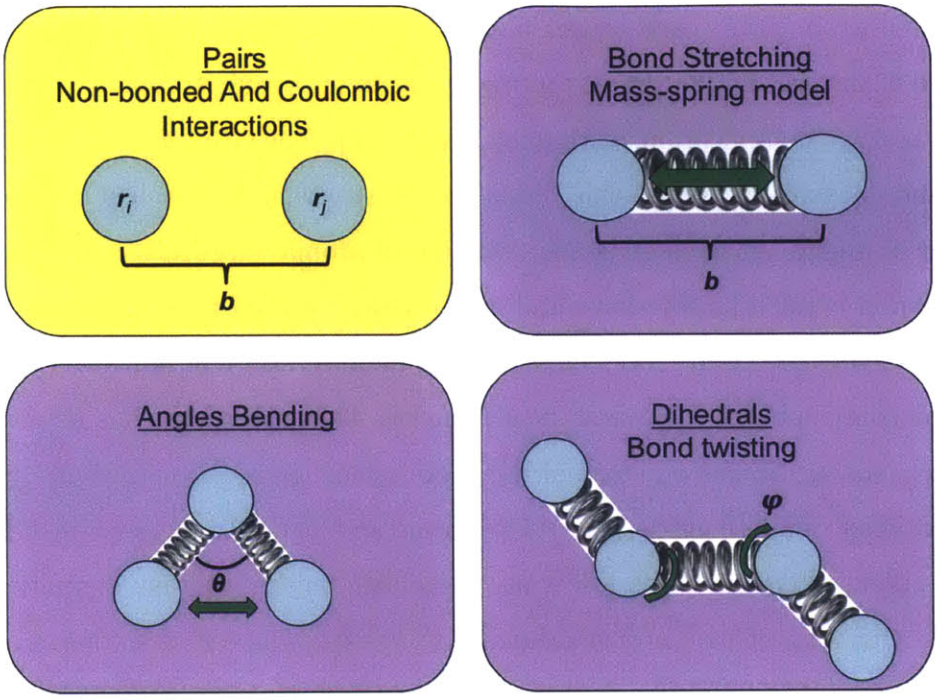

Figure 2-3: Diagrams of the GROMOS 53A6 atomic interactions used in the bulk octane system. The light blue spheres represent the atoms involved in the interaction and the springs represent chemical bonds. The yellow background denotes intermolecular interactions and the purple backgrounds are intramolecular interactions. Pairs interactions include the non-bonded interactions (also commonly known as van der Waals interactions) and coulombic interaction. Dihedral interactions are due to bonds twisting, and the angle φ measures the displacement of the twisting from equilibrium.

used in this work to model covalent bond stretching because the form of E_b^{GROMOS} is not currently supported by LAMMPS. The latest version of LAMMPS used in this work is the release on Feb. 1, 2014. The harmonic bond interaction does not lead to an infinite thermal conductivity in the bulk octane system (which is clearly unphysical) because the overall system is anharmonic due to the other atomic interactions and couplings between different interactions. Even though each type of atomic interaction is harmonic, they depend on different displacements, which make the system anharmonic. The reason can be easily seen by considering bond stretching and angles angles. The energy for bond stretching and angles bending are given in equation (2.4) and equation (2.5), respectively. The energies just due to bond stretching, E_b, is har-

monic with respect to the displacement r while the energies just due to bond bending, E_a, is harmonic with respect to the cosine of the displacement angle θ. However, the sum of E_b and E_a will depend on both r and $cos\theta$, which introduces anharmonic effects.

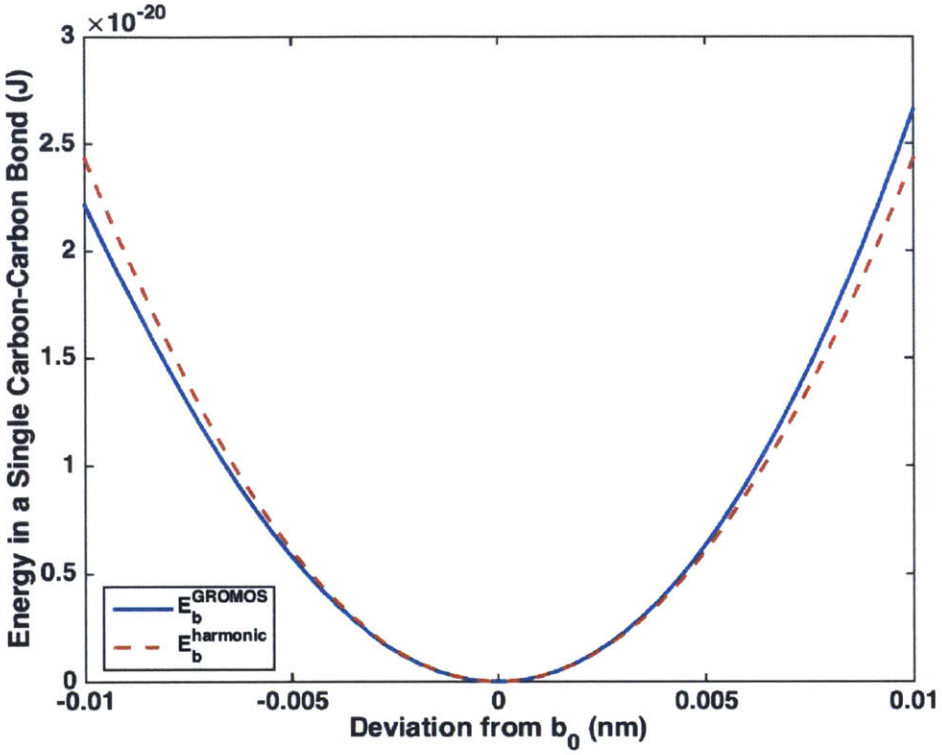

Figure 2-4: Comparison between E_b^{GROMOS} and $E_b^{harmonic}$ for a single carbon-carbon bond being displaced from the equilibrium length $b_0 = 0.11$ nm. The typical amplitude for atomic vibrations is on the order of 0.01 nm [57]. Within this range, the difference between E_b^{GROMOS} and $E_b^{harmonic}$ is less than 5%.

Angle interactions in octane occur between three atoms, i, j, and k, that are linked by two covalent bonds. Potential energy due to bending of the angle formed by the two covalent bonds is

$$E_a^{GROMOS} = \sum_{n=1}^{N_a} \frac{1}{2} K_{an}^{GROMOS} \left[cos(\theta_n) - cos(\theta_{0n})\right]^2 \tag{2.5}$$

where K_{an}^{GROMOS} is like the spring constant for bending the nth angle, θ_n is the measurement of the nth angle, and θ_{0n} is the equilibrium value of the nth angle. The functional dependence on $cos(\theta_n)$ rather than θ_n reduces computational costs by eliminating an arccosine operation that the purely harmonic form

$$E_a^{harmonic} = \sum_{n=1}^{N_a} K_{an}^{harmonic} [\theta_n - \theta_{0n}]^2 \tag{2.6}$$

would require.

The torsional dihedral term describes interactions from bonds twisting. The energy is given by

$$E_d^{GROMOS} = \sum_{n=1}^{N_d} K_{dn}^{GROMOS} [1 + cos(\delta_n) cos(m_n \varphi_n)] \tag{2.7}$$

where δ_n is the phase shift (restricted to 0 or π), m_n is the multiplicity of the torsional dihedral, φ_n is the actual value of the dihedral angle. The trans configuration is defined as $\varphi_n = 0$. The restriction on δ_n allows E_d^{GROMOS} to be rewritten in the harmonic form

$$E_d^{harmonic} = \sum_{n=1}^{N_d} K_{dn}^{harmonic} [1 + d_n \, cos(m_n \varphi_n)]] \tag{2.8}$$

where $K_{dn}^{harmonic} = K_{dn}^{GROMOS}$, $d_n = +1$ for $\delta_n = 0$ and $d_n = -1$ when $\delta_n = \pi$.

Non-bonded interactions are modeled in GROMOS by the sum of Lennard-Jones potential [15] and electrostatic interactions. The form of the Lennard-Jones potential used is

$$E_{LJ} = \sum_{pairs \; i,j} \left[\frac{C_{12ij}}{r_{ij}^{12}} - \frac{C_{6ij}}{r_{ij}^{6}} \right] \tag{2.9}$$

where C_{12ij} and C_{6ij} are parameters describing the strength of the pairs interaction

and r_{ij} is the separation betweens atoms i and j. In theory, all pairs of atoms should be considered in the sum. In practice, atoms connected with covalent bonds are typically excluded from the sum because their interaction is already considered by the bond term. Additionally, atoms further than the cutoff distance are not considered in the sum to reduce computational time as discussed in section 2.1. The Lennard-Jones form is also commonly written as

$$E_{LJ} = 4\epsilon \left[\left(\frac{\sigma}{r}\right)^{12} - \left(\frac{\sigma}{r}\right)^{6} \right] . \tag{2.10}$$

In this form, the physical interpretation of the parameters ϵ and σ is much clearer (see figure 1-3). ϵ can be identified as the minimum energy and σ as the minimum energy length scale with $C_{12ij} = 4\epsilon_{ij}\sigma_{ij}^{12}$ and $C_{6ij} = 4\epsilon_{ij}\sigma_{ij}^{6}$. Physically, the r_{ij}^{-6} term describes attraction between two atoms at long ranges due to non-bonded interactions and is derived from quantum mechanics for instantaneous dipole-dipole interactions. The r_{ij}^{-12} term describes repulsion at close distances, which prevents atoms from occupying the same space. The selection of r^{-12} is not justified through any physical argument, but is historically used for numerical simplicity since it is easily calculated as the square of r^{-6}. Using r^{-12} exponent reproduces a sufficiently accurate approximation to the repulsion from overlapping electron orbitals, but other large repulsive terms, such as r^{-13} or r^{-14} [58] or exponentials of the form e^{-Kr}, where K is a positive constant [59] will generally not significantly impact the MD results. Electrostatic interactions are modeled with the familiar

$$E_{electrostatic} = \sum_{pairs\ i,j} \frac{1}{4\pi\epsilon_0\epsilon_1} \frac{q_i q_j}{r_{ij}} , \tag{2.11}$$

where ϵ_0 is the dielectric permittivity of the vacuum, ϵ_1 is the relative permittivity of the medium in which the atoms are embedded, r_{ij} is the distances between atoms i and j , and q_i, q_j are the charges on atoms i and j respectively. It is standard to set the value of ϵ_1 to 1 since MD systems are typically constructed as atoms in a vacuum,

as is the case in the bulk octane system. Alkane molecules are typically non-polar, but partial charges do exist on some hydrogen and carbon atoms due to the large difference in electronegativities of these two elements. The molecule is charge neutral overall. Both the Lennard-Jones and electrostatic potentials are pairs interactions; that is, they describe the interactions between a pair of atoms. In the rest of the work, the term "pairs interactions" will refer to the sum of Lennard-Jones and electrostatic interactions. The energy due to the pairs interactions is defined as

$$E_p = E_{LJ} + E_{electrostatic} \ . \tag{2.12}$$

It is also useful to note that the pairs interactions act on atoms that are not connected with chemical bonds; these are the interactions that can carry heat from one molecule to another molecule and are thus the intermolecular interactions. Likewise, it is useful to group bond, angle, and dihedral interactions, which require atoms to be chemically bonded and thus belong to the same molecule, as the intramolecular interactions.

2.3 System Convergence

Once information about the atomic structure and interactions are obtained, there are generally four steps to an MD simulation: 1) convergence, 2) minimization, 3) equilibration, and 4) production run. The first three steps are required to ensure that the last step is a good model for the physical system being studied and produces correct results. Each of the steps will be described in the next several sections.

The first step, system convergence, is a critical issue for all numerical simulations, not just MD. This step ensures that data collected during the simulation is a true representation of the conditions under investigation rather than artifacts due to ap-

proximations made in the simulation process. MD makes two main approximations in modeling the bulk system: finite time steps and finite system size. Thus, it is imperative to check these approximations are accurate enough to produce correct results. Specifically, MD is modeling a continuous process (the atomic movements) as a series of time steps and integrating velocities to find the new positions. As such, the time step size is critical for obtaining accurate results. If the step is too big, then the phenomenon under study may not appear. Additionally, big time steps can lead to large integration errors and unstable systems because atoms are allowed to move too far apart. However, if the time step is too small, then more steps will be needed to reach the desired total simulated time, thus requiring more computational power. In general, a good rule of thumb is to start with a time step an order of magnitude smaller than the frequency of the fastest atomic vibration in the system and test for convergence from there.

Clever time integration methods can reduce the error and allow the use of larger time steps. The velocity Verlet method [60], the default integrator in LAMMPS, is widely used to reduce the time integration errors, and gives much more satisfactory results than the simple Euler method discussed in section 2.1. In the velocity Verlet method, the position of an atom at the end of the time step is calculated as

$$\mathbf{r}_{t+dt} = \mathbf{r}_t + \mathbf{v}_t \cdot dt + \frac{1}{2}\mathbf{a}_t \left(dt\right)^2 \tag{2.13}$$

where $\mathbf{r}$ is the position, $\mathbf{v}$ is the velocity, dt is the time step size, and $\mathbf{a}$ is the acceleration. The subscripts t and $t+dt$ denotes the value before and after taking the time step, respectively. Then, $\mathbf{a}_{t+dt}$ is calculated using Newton's law $\mathbf{F} = m\mathbf{a}$, with $\mathbf{F}$ determined by the position $\mathbf{r}_{t+dt}$ and the atomic interactions. Next, the velocity at the end of the time step is calculated as

$$\mathbf{v}_{t+dt} = \mathbf{v}_t + \frac{\mathbf{a}_t + \mathbf{a}_{t+dt}}{2} dt \ . \tag{2.14}$$

In this method, the accelerations at the beginning of the time step $\mathbf{a}_t$ and the velocity at the end of the time step $\mathbf{a}_{t+dt}$ are averaged when calculating the new velocity. This correction gives significant improvements over the simple Euler method described in equations (2.1) and (2.2).

The size of the the base cell used with periodic boundary conditions is vitally important to reach system size convergence. The periodic boundary condition creates an infinite system with finite degrees of freedom, so convergence ensures that there are enough degrees of freedom to accurately calculate the properties under investigation. In crystalline solids, the cell can be relatively small, since the real bulk system is actually periodic. In liquids and gases, however, the base cell must be much larger because there is no periodicity in these materials and the cell must be big enough that the periodicity caused by the periodic boundary condition has negligible effect.

Since liquid molecules have no periodic order, it is tempting to start the calculation with molecules randomly placed within the simulation box. However, doing so can lead to unrealistic configurations if atoms start out too close to each other. Instead, it is more advisable to start with molecules in an ordered configuration with the correct density and then run a long minimization step to randomize the molecule placement. One may also be tempted to check that molecules are sufficiently randomized only with visuals, but this can be deceiving. Instead, the molecular positions should be plotted to make sure the system is sufficiently randomized.

2.4 Minimization

After the appropriate time step size and system size has been found, the next step is to minimize the energy within the system. Typically, the initial atomic structure used in the calculations is not actually the optimal stable structure, but a guess at what

that structure would be. Therefore, the stable structure must be found by allowing the atoms to move to more stable (i.e. lower energy) configurations. Minimization, by itself, provides a great deal of information about the system. For example, in biology, finding the minimum energy configuration in proteins is at the heart of studies on finding protein structures. As the many massive-scale distributed computing programs, such as Folding at Home [61], demonstrate, finding the minimum energy configuration for a system is not a trivial task. When starting calculations for system dynamics, however, it is imperative to first find a minimum in the energy surface to serve as a stable starting point. The minimized system is the configuration about which fluctuations occur during the time trajectory of the system. The fluctuations, in turn, provide the dynamics that are the underpinning of MD. The net force on each atom is zero at a minimum energy point, and a system may have more than one local minimum. Typically, the local minimum can be found fairly easily by using well-developed protocols, but finding the global minimum requires a scan of the conformational space. For dynamics calculations, it is typically not necessary (and extremely challenging given the the typical system size) to find the global minimum. There are three commonly used methods for minimizing the system energy: 1) steepest descent [62], 2) conjugate gradient [63], and 3) Newton-Raphson [64]. The steepest descent method, although robust, is not especially efficient computationally. Nevertheless, it is sufficient for this work.

The steepest decent finds the energy minimum by following the negative of the first derivative. For a potential surface, E, the minimization starts with a guess at the local minimum, $\mathbf{x}_1$. Then, a second point on the energy surface, $\mathbf{x}_2$, is found by taking a small step δ in the direction of the negative gradient of E so that

$$\mathbf{x}_2 = \mathbf{x}_1 - \delta \nabla E\left(x_1\right) \tag{2.15}$$

$$\text{and } E\left(\mathbf{x}_2\right) \leq E\left(\mathbf{x}_1\right) \ . \tag{2.16}$$

Subsequent steps $\mathbf{x}_3$, $\mathbf{x}_4$, ... are found in the same manner to generate a path $E(\mathbf{x}_1) \geq E(\mathbf{x}_2) \geq E(\mathbf{x}_3) \geq E(\mathbf{x}_4) \geq \ldots$ that leads to the lowest energy configuration. Note that δ can change at every step but arbitrary values of δ will not ensure convergence.

The line search method is one way to determine δ that is guaranteed to reach a local energy minimum. In this method, a line is drawn from an initial guess using the gradient of E until the line reaches another point at the same energy. The starting point for the next guess is taken to be the point along the line with the minimum energy. Consider a simple, 2D potential energy surface example:

$$E(x, y) = 2x^2 + 5y^2 \quad . \tag{2.17}$$

The minimum of E, of course, is located at $(0, 0)$. The gradient is

$$\nabla E = (4x, 10y) \quad . \tag{2.18}$$

The line used for finding the second point given an initial guess (x_1, y_1) is

$$x_1' = x_1 + \delta \left(\frac{\partial E}{\partial x}\right)\Big|_{x_1, y_1} = x_1 (1 + 4\delta) \tag{2.19}$$

$$y_1' = y_1 + \delta \left(\frac{\partial E}{\partial y}\right)\Big|_{x_1, y_1} = y_1 (1 + 10\delta) \quad . \tag{2.20}$$

Equations (2.19) and (2.20) form a set of parametric equations for a line going through the potential surface, E. This line also goes through another point with $E(x_1', y_1') = E(x_1, y_1)$. Between (x_1, y_1) and (x_1', y_1'), the energy E is lower than $E(x_1', y_1') = E(x_1, y_1)$ so there must a minimum energy point on the line. This point is taken to be (x_2, y_2). The same procedure is then used to find (x_3, y_3) and subsequent points until arriving at the local minimum. This example, illustrated in figure 2-5, though trivially simple, illustrates the method for energy minimization through following the

gradient of the energy. In this example, the minimum is found fairly quickly because the potential energy surface is quadratic. For an MD system, there are many more degrees of freedom and additional complexities, but the principle is the same as this example. Energy minimization algorithms are typically built into MD software, as is the case for LAMMPS, since they are vital to the simulation; all the user has to do is call up the appropriate commands in the input script.

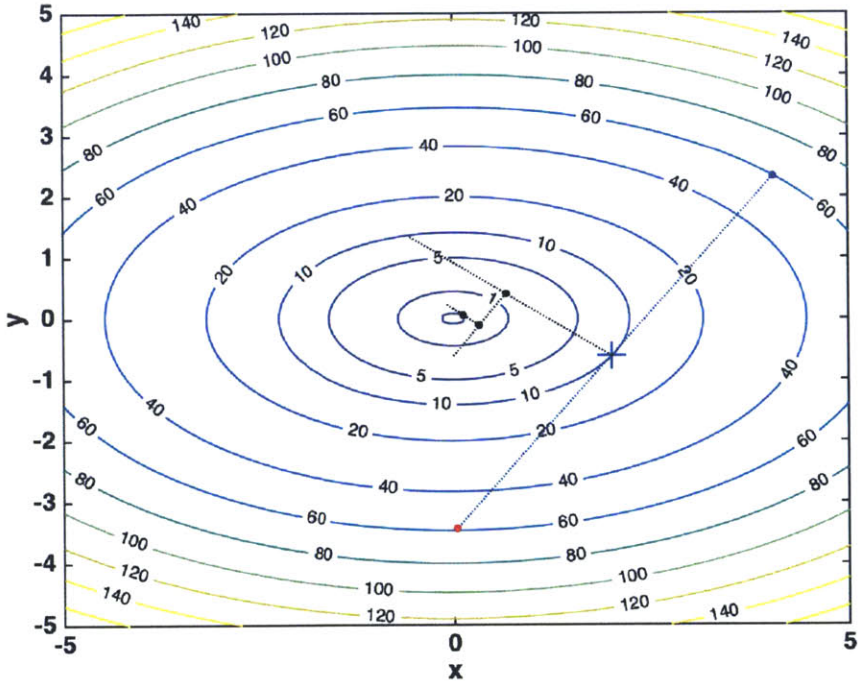

Figure 2-5: An simple example illustrating the principle of steepest descent minimization. The potential energy surface is $E(x, y) = 2x^2 + 5y^2$. The minimum, of course, is located at $(0, 0)$. An initial guess of $(x_1, y_1) = (4.05, 2.33)$, marked by the blue dot, starts the numerical search for a local minimum. $E(4.05, 2.33) = 60$. The line search for (x_2, y_2) proceeds along the dotted blue line, parametrized by $x_1' = x_1(1 + 4\delta)$, $y_1' = y_1(1 + 10\delta)$, and intersects the contour $E = 60$ at another point $(0.04, -3.44)$, marked with a red dot. Thus the minimum of E on the dotted blue line must be between (4.05, 2.33) and (0.04, -3.44). This point, marked with a blue $+$, is $(x_2, y_2) = (2.01, -0.61)$. The next line search starts at $(x_2, y_2) = (2.01, -0.61)$ and yields $(x_3, y_3) = (0.67, 0.41)$. The rest of the search path is shown, ending at $E(0.12, 0.06) = 0.05$ after two more steps.

2.5 Equilibration, Thermostats, and Barostats

Once a local minimum energy configuration has been found, the work of creating a statistically accurate MD representation of the system under investigation can begin in earnest. The next step is equilibrating the system to reach the desired temperature and pressure conditions through use of a thermostat or barostat. In addition to randomizing molecule locations, equilibration serves the more important purpose of properly distributing the total energy between potential and kinetic and adjusting energies within the system to maintain the desired temperature or pressure even when thermostats and barostats are removed from the equations of motion.

The basic MD equations describe velocity, acceleration, and forces through time and do not contain direct temperature information. However, one can use the kinetic energy distribution to calculate the temperature. The simple way is to first calculate the average kinetic energy and then apply the equipartition theorem. The total kinetic energy, E_K, of the system is

$$E_K = \frac{1}{2}\sum_{i=1}^{N} m_i v_i^2 \tag{2.21}$$

where m_i is the mass of ith atom, v_i is the magnitude of the velocity of the ith atom, and N is the total number of atoms in the system. From the equipartition theorem, each mode of freedom with a quadratic potential contributes $\frac{1}{2}k_BT$, where k_B is the Boltzmann constant, and T is the temperature, to the total energy. Kinetic energy has a quadratic potential and 3 degrees of freedom, along the x, y, or z axis, so the kinetic energy of a single atom is $\frac{3}{2}k_BT$ and that of the full system is

$$E_K = \frac{3}{2}Nk_BT \tag{2.22}$$

where N is the total number of atoms in the system. Setting the two expressions for

E_K equal yields

$$E_K = \frac{1}{2}\sum_{i=1}^{N} m_i v_i^2 = \frac{3}{2} N k_B T \tag{2.23}$$

$$\Rightarrow T = \frac{1}{3Nk_B}\sum_{i=1}^{N} m_i v_i^2 \ . \tag{2.24}$$

In calculating v_i, the center of mass of the system must be set to zero. If the center of mass moves, the center of mass velocity must be subtracted from the velocity of each atom.

Often, it is necessary to generate velocities for the atoms to start the simulation and desirable to have the initial velocities match a particular temperature. This can be accomplished by creating initial velocities for the atoms in the system using the Maxwell-Boltzmann distribution. The Maxwell-Boltzmann distribution gives the probability of finding an atom with a particular velocity component within the system. For the x component of velocity, v_x,

$$\rho(v_x) = \sqrt{\frac{m}{2\pi k_B T}} e^{-\frac{m v_x^2}{2 k_B T}} \ . \tag{2.25}$$

Note that $\rho(v_x) = \rho(v_y) = \rho(v_z)$ is a Gaussian distribution with mean of 0 and variance of $\sigma^2 = \frac{k_B T}{m}$. The necessary temperature distribution can then be easily created by using a random number generator to create a set of velocities that satisfy the Maxwell-Boltzmann distribution. Even with velocity generated in this way, it is still necessary to equilibrate the system to reach a reasonable minimum energy configuration.

The basic MD formulation is a description for the microcanonical ensemble: the system is completely isolated. In MD, the microcanonical ensemble is often called the NVE ensemble, where N refers to the number of atoms, V to the volume of the system, and E to the total system energy, since N, V, and E are held constant. However,

most physical systems are not isolated. Instead, typically either the temperature and/or pressure is held constant instead of the total energy. These are the NVT and NPT ensembles, respectively. Thermostats and barostats required in NVT and NPT ensembles to maintain the desired temperature and/or pressure.

The expression for system temperature in equation (2.24) suggests a simple way to maintain a constant temperature. At each time step, the velocities of the atoms can be rescaled by multiplying each velocity with a factor λ. This procedure produces the desired temperature as

$$\begin{aligned} T_{desired} &= \frac{1}{3Nk_B} \sum_{i=1}^{N} m_i \left(\lambda v_i\right)^2 \\ &= \frac{\lambda^2}{3Nk_B} \sum_{i=1}^{N} m_i v_i^2 \\ &= \lambda^2 T \\ \lambda &= \sqrt{\frac{T}{T_{desired}}} \end{aligned} \tag{2.26}$$

where T is the temperature before rescaling. If the temperature is too high, this method takes some energy out of the system by slowing all the atoms down, and if the temperature is too low, this method adds energy by increasing the velocities. This rescaling enforces the desired temperature at every time step so that if the desired temperature is far away from the current system temperature, rescaling by λ will introduce large temperature fluctuations accompanied by large over or under-shooting. Furthermore, this rescaling does not allow for *any* fluctuations in system temperature, which may not be physical.

The Berendsen thermostat [65] solves much of the issues with the velocity rescaling

method by changing the velocity slowly over many time steps such that

$$\frac{dT}{dt} = \frac{1}{\tau}\left(T_{desired} - T\right) \tag{2.27}$$

where τ controls how quickly the temperature is changed. The change in temperature at each time step is

$$\delta T = \frac{\delta t}{\tau}\left(T_{desired} - T\right)$$

where δt is the size of the time step. Then, the required velocity scaling parameter $\lambda_{Berendsen}$ is calculated as

$$\delta T = \lambda_{Berendsen}^2 T - T = \frac{\delta t}{\tau}\left(T_{desired} - T\right) \tag{2.28}$$

$$\lambda_{Berendsen} = \sqrt{1 + \frac{\delta t}{\tau}\left(\frac{T_{desired}}{T} - 1\right)}\ . \tag{2.29}$$

Note that if $\tau = \delta t$, $\lambda_{Berendsen}$ reduces to the simple rescaling parameter in equation (2.26) and the Berendsen method becomes the simple velocity rescaling discussed previously. In contrast, as $\tau \to \infty$, $\lambda_{Berendsen} \to 1$ so the velocity is no longer being rescaled and the system reduces to the microcanonical ensemble.

The pressure of the system can be calculated from

$$P = \frac{N k_B T}{V} + \frac{\sum_i^N \mathbf{r}_i \cdot \mathbf{f}_i}{dV} \tag{2.30}$$

where P is the system pressure, V is the system volume, $\mathbf{r}_i$ is the position of the ith atom, $\mathbf{f}_i$ is the force on the ith atom, and d is the number of dimensions in the system [66]. For a bulk system, $d = 3$. Note that the first term of equation (2.30) is the familiar ideal gas law and the second term is a viral correction to account for atom interactions. Similarly to temperature, the expression for pressure suggests a simple

way to adjust the system pressure during calculations: by changing V. The system volume can be adjusted by length scaling to change the system pressure, P, to the desired pressure, $P_{desired}$, similar to scaling the atom velocity to change the system temperature. For a cubic system, the volume of the system and the length of the system, l, is related by $V = l^3$, so the scaling becomes

$$V = l^3 \rightarrow \mu^3 l^3 \tag{2.31}$$

$$\mathbf{r}_i \rightarrow \mu \mathbf{r}_i \ . \tag{2.32}$$

As in thermostating, the Berendsen method provides a way of slowly adjusting the volume towards the desired pressure. The Berendsen scaling factor is

$$\mu_{Berendsen} = \left[1 - \frac{\beta \delta t}{\tau_P} \left(P_{desired} - P\right)\right]^{1/3} \tag{2.33}$$

where β is the isothermal compressibility. This choice for scaling factor satisfies

$$\frac{dP}{dt} = \frac{1}{\tau_P} \left(P_{desired} - P\right) \tag{2.34}$$

ensuring the system exponentially decays towards the desired pressure. The exact isothermal compressibility for the system is not required to apply the Berendsen barostat since β appear only in a ratio to τ_P, the pressure relaxation timescale.

The Berendsen thermostat in conjunction with the Berendsen baraostat give realistic fluctuations in temperature and pressure [65] and are extremely efficient for relaxing the system to the desired temperature and pressure. However, they do not produce canonical distributions. Other methods, notably Nose-Hoover [67, 68], have been developed and proven to accurately reproduce equilibrium canonical statistics. The Nose-Hoover thermostat changes the equations of motion to include a heat bath that is used to maintain the system at the desired temperature. Then, the extended system (heat bath and original system) forms a microcanonical ensemble while the original

system correctly produces equilibrium canonical behavior. Since the Green-Kubo formulas are derived under the assumption of canonical ensembles, the Nose-Hoover thermostat is often used to enforce an NVT ensemble during the production run. However, the Nose-Hoover thermostat has only been proven to produce the correct *equilibrium* canonical statistics, and no thermostat has been proven to produce the correct *dynamical* properties [69], such as the heat flux correlation functions used in the Green-Kubo method. Instead, the heat flux correlation functions should be evaluated by averaging multiple NVE runs from systems that have been carefully relaxed to equilibrium in NVT.

Every time the system temperature and pressure is adjusted through the thermostats, the system will be out of equilibrium. Additional time steps are required to bring the system back into equilibrium. Note that this equilibrium refers to the dynamic equilibrium, not the minimum energy equilibrium configuration found during minimization. A well equilibrated system will keep fairly constant pressure and temperature even without additional constraints from thermostats and barostats. This allows an NVE ensemble to produce the canonical distributions required for Green-Kubo. It is a good practice to switch between NVT and NPT ensembles several times during equilibration and, before starting the production run, to confirm that the system is indeed well equilibrated with a NVE equilibration segment.

Chapter 3

MD Calculation Analysis

Molecular dynamics calculates the trajectories of and the forces acting on each atom through time. These two sets of data can then be used to calculate macroscopic properties of the system. This chapter will introduce the methods for connecting atomic trajectories and forces to thermal conductivity. Thermal conductivity can be calculated using non-equilibrium MD by imposing a temperature difference between opposite sides of the system, calculating the heat flux across the system, and fitting to Fourier's Law $q = -k\frac{dT}{dx}$, where q is the heat flux, k is the thermal conductivity, T is the temperature, and x is in the direction of the temperature gradient [20]. The second method for non-equilibrium MD is to impose a heat flux, calculate the resultant temperature gradient, and fit to Fourier's Law [21]. Alternatively, the Green-Kubo formula can be used to calculate thermal conductivity in an equilibrium system [19]. This method relies on natural fluctuations in the equilibrated system, so the noise to data ratio is larger than the non-equilibrium method. This work uses equilibrium MD and the Green-Kubo formula because the temperature gradient or heat flux required in non-equilibrium MD is typically larger than would naturally occur in the system [70] and are therefore not physical. This chapter will first discuss how heat flux is

calculated, and then will develop several equations that will later be used to analyze the MD data.

3.1 Stress and Heat Flux

As discussed in chapter 2, MD calculations only require calculating atomic trajectories (positions and velocities) and forces, but these two sets of data can be used to calculate many other properties. Calculating stress on each atom from velocities and forces is straightforward. Then, the stresses can be used to calculate heat flux on each atom. In LAMMPS, the stress on an atom A is defined as

$$\begin{aligned} S_{ij} = -\frac{1}{V}\Big[& mv_i v_j + \frac{1}{2}\sum_{n=1}^{N_p}(r_{n1i}F_{n1j} + r_{n2i}F_{n2j}) \\ & + \frac{1}{2}\sum_{n=1}^{N_b}(r_{n1i}F_{n1j} + r_{n2i}F_{n2j}) + \frac{1}{3}\sum_{n=1}^{N_a}(r_{n1i}F_{n1j} + r_{n2i}F_{n2j} + r_{n3i}F_{n3j}) \\ & + \frac{1}{4}\sum_{n=1}^{N_d}(r_{n1i}F_{n1j} + r_{n2i}F_{n2j} + r_{n3i}F_{n3j} + r_{n4i}F_{4j}) + \cdots \Big] \end{aligned} \tag{3.1}$$

where S is the stress component, V is the volume occupied by the group of atoms considered, m is the mass of the atom, v_i and v_j are velocity components, r is the positions of the atoms involved in the interaction, and F is the force acting on the atoms due to the interaction [66]. The indices i, j rotates between x, y, and z to produce the components of the symmetric stress tensor. Additional interactions not used in the octane system are not shown. The total stress is the sum of the kinetic energy contribution (the first term) and each type of atomic interactions, where p stands for pairs interactions, b stands for bonds stretching, a stands for angles bending, and d stands for dihedral interactions. The subscripts $n1$, $n2$, $n3$, and $n4$ refers to the different atoms involved with the nth instance of each type of interaction. There can be more than one instance of each type of interaction acting

on atom A. N_p, N_b, N_a, and N_d are the number of pairs, bonds stretching, angles bending, and dihedral interactions atom A participates in. For example, A could could be part of two bonds: one with atom B and the other with atom C. Then, $N_b = 2$ and the stress components on A from bond stretching is the sum of those two bonds and equals

$$\begin{aligned}\frac{1}{2}\sum_{n=1}^{N_b}\left(r_{n1i}F_{n1j} + r_{n2i}F_{n2j}\right) &= \frac{1}{2}\left(r_{11i}F_{11j} + r_{12i}F_{12j}\right) + \frac{1}{2}\left(r_{21i}F_{21j} + r_{22i}F_{22j}\right) \\ &= \frac{1}{2}\left(r_{Ai}F_{Aj} + r_{Bi}F_{Bj}\right) + \frac{1}{2}\left(r_{Ai}F_{Aj} + r_{Ci}F_{Cj}\right) \ .\end{aligned} \tag{3.2}$$

Note the coefficients before the sums in equation (3.1). The stress due to interactions involving a group of atoms (i.e. 2 atoms for pairs and bond interaction, 3 for angle interactions, and 4 for dihedral interactions) is split evenly between the atoms involved. This method for calculating stress is essentially the virial stress [71]. From the stress tensor $\mathbf{S}$, heat flux $\mathbf{J}$ over a group of n atoms can be calculated as

$$\mathbf{J} = \frac{1}{V}\left[\sum_{i}^{n} K_i\mathbf{v}_i + \sum_{i}^{n}\phi_i\mathbf{v}_i\right] - \sum_{i}^{n}\mathbf{S}_i\mathbf{v}_i \ , \tag{3.3}$$

where V is the volume occupied by the n atoms, K_i is the kinetic energy of the ith atom, ϕ_i is the potential energy of the ith atom, and $\mathbf{v}_i$ is the velocity [66].

3.2 The Green-Kubo Equation for thermal conductivity

Evaluating correlation functions reveal underlying dynamical processes in a molecular system. The heat flux correlation function is defined as

$$C_{\mathbf{J}}(t) = \langle \mathbf{J}(0)\cdot\mathbf{J}(t)\rangle \ . \tag{3.4}$$

This is constructed for any atomic trajectory by setting the chosen initial time step to $t = 0$. The $\langle\ \rangle$ signals ensemble average, meaning that $C_{\mathbf{J}}$ is the average over the full system. For an MD system at an equilibrium temperature, there will be fluctuations in local temperature due to statistical variations through the system. This leads to local heat fluxes. The correlation function shows how quickly local heat flux influences the rest of the system. For a system that does not interact with itself, $\mathbf{J}(t)$ will not change with respect to time and $C_{\mathbf{J}}$ will be constant. As the system starts to interact with itself, $\mathbf{J}(t)$ will gradually change due to influences from the other molecules in the system. In this case, the correlation between $\mathbf{J}(t)$ and $\mathbf{J}(t = 0)$ will get smaller as time goes on, and $C_{\mathbf{J}}$ will decay towards zero. As the system interaction gets stronger, $\mathbf{J}(t)$ begins to oscillate since heat can transfer easily in both directions of an interaction, and $C_{\mathbf{J}}$ will reflect those oscillations. However, the peak of each oscillation will get smaller, similar to a damped oscillator. The correlation function of $\mathbf{J}$ indicates how much the heat flux in the system at the current time depends on the heat fluxes at an earlier time and can be used to calculate the thermal conductivity of the system. In systems with high thermal conductivity, heat in one location will quickly influence surrounding areas so the correlation will be high. In systems with low thermal conductivity, heat in one location influences surrounding areas much more slowly so the correlation is low.

The Green-Kubo equations formally connects flux correlations to transport coefficients. They form the basis for calculating dynamic system properties in equilibrium molecular dynamics. For thermal conductivity, κ, the Green-Kubo equation is:

$$\kappa = \frac{V}{3k_B T^2} \int_0^\infty \langle \mathbf{J}(0) \cdot \mathbf{J}(t) \rangle dt \ . \tag{3.5}$$

This equation can be derived using the Liouville equation in linear response theory [70]. The linear response theory simplifies the response of a system to external perturbations to a linear relationship. In many cases, real systems do not respond to

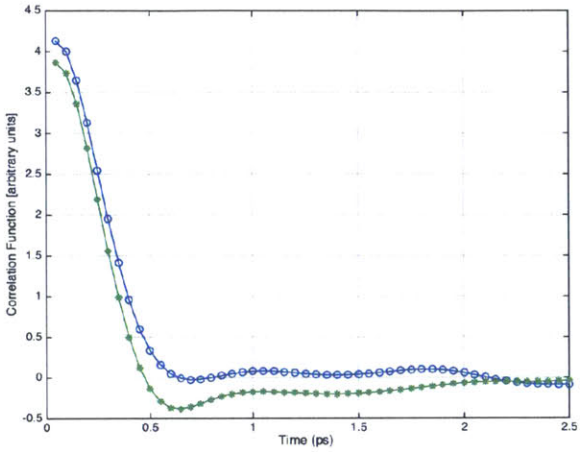

Figure 3-1: Comparison between a system with strong correlations and weak correlations. The strongly correlated system, shown in green and marked with asterisks, has oscillations that persist far longer than the weakly correlated system, shown in blue and marked with circles.

external applied fields linearly, but as the perturbations become small, this description becomes accurate. The Liouville equation is

$$0 = \frac{\partial f^{(N)}}{\partial t} + \sum_{i}^{n} \frac{\partial H}{\partial p_i} \frac{\partial f^{(N)}}{\partial r_i} - \sum_{i}^{n} \frac{\partial H}{\partial r_i} \frac{\partial f^{(N)}}{\partial p_i} \tag{3.6}$$

where $f^{(N)}$ is the N particle distribution function and

$$H\left(\mathbf{r}, \mathbf{p}\right) = \frac{1}{2m} \sum_{i}^{n} p_i^2 + U(\mathbf{r}) \tag{3.7}$$

is the Hamiltonian of the system. $\mathbf{p}$ is the generalized momentum of the N particles and $U(\mathbf{r})$ is a potential energy dependent on the locations, $\mathbf{r}$, of the N particles. The summation $\sum_i^n$ acts over the components of the generalized coordinates $(\mathbf{r}, \mathbf{p})$. This equation describes the time evolution of the phase space distribution function and satisfies conservation of phase space density. The Poisson bracket $\{A, B\}$ is

commonly used to simplify notation and is defined as

$$\{A, B\} \equiv \sum_{i}^{n} \left(\frac{\partial A}{\partial r_i} \frac{\partial B}{\partial p_i} - \frac{\partial A}{\partial p_i} \frac{\partial B}{\partial r_i} \right) \tag{3.8}$$

where A and B are arbitrary functions of the phase space variables. The Liouville operator, Γ, is defined as

$$\Gamma g \equiv i\{H, g\} \tag{3.9}$$

where g is any function and $i = \sqrt{-1}$ is the imaginary number. Using equations (3.8) and (3.9), the Liouville equation can be re-written as

$$\begin{aligned} \frac{\partial f^{(N)}}{\partial t} &= \{H, f^{(N)}\} \\ &= -i\Gamma f^{(N)} \ . \end{aligned} \tag{3.10}$$

Linear response theory assumes that Γ does not explicitly depend on time [72] so the solution to equation (3.10) is of the form

$$f^{(N)}(\mathbf{r}, \mathbf{p}, \mathbf{t}) - f^{(N)}(\mathbf{r}, \mathbf{p}, \mathbf{0})\, e^{-it\Gamma} \ . \tag{3.11}$$

For a small disturbance, we can write $f^{(N)} = f_o^{(N)} + f_\delta^{(N)}$ and $H = H_o + H_\delta$. Then, the Liouville equation becomes

$$\begin{aligned} \frac{\partial f_o^{(N)}}{\partial t} + \frac{\partial f_\delta^{(N)}}{\partial t} &= \{H_o + H_\delta, f_o^{(N)} + f^{(N)}\} \\ &= \{H_o, f_o^{(N)}\} + \{H_o, f_\delta^{(N)}\} + \{H_\delta, f_o^{(N)}\} + \{H_\delta, f_\delta^{(N)}\} \ . \end{aligned} \tag{3.12}$$

Assuming the last term is small, since both H_δ and $f_\delta^{(N)}$ are small, equation (3.12)

can be simplified, and $\frac{\partial f_\delta^{(N)}}{\partial t}$ identified as

$$\begin{aligned}
\frac{\partial f_o^{(N)}}{\partial t} + \frac{\partial f_\delta^{(N)}}{\partial t} &= \{H_o, f_o^{(N)}\} + \{H_o, f_\delta^{(N)}\} + \{H_\delta, f_o^{(N)}\} \\
\frac{\partial f_o^{(N)}}{\partial t} &= \{H_o, f_o^{(N)}\} \\
\frac{\partial f_\delta^{(N)}}{\partial t} &= \{H_o, f_\delta^{(N)}\} + \{H_\delta, f_o^{(N)}\} \qquad (3.13)
\end{aligned}$$

The probability distribution in a canonical system with a small temperature disturbance, δT, is

$$f = Ce^{-\frac{h\Delta V}{k_B(T+\delta T)}} \qquad (3.14)$$

$$\approx Ce^{-\frac{h\Delta V}{k_B T}\left(1-\frac{\delta T}{T}\right)} \qquad (3.15)$$

where C is a normalization constant, h is the local energy density, k_B is the Boltzmann constant, and ΔV is the local volume [72]. The approximation is derived by using the Taylor expansion $\frac{1}{1+x} = 1 - x + x^2 - x^3 + \ldots$ around $x = 0$. Then, the corresponding local energy disturbance, to the first order, is $-h\Delta V\frac{\delta T}{T}$, and the perturbed Hamiltonian can be written as

$$H = H_o + H_\delta \approx H_o - \int h(\mathbf{r}(t))\frac{\delta T(\mathbf{r})}{T} dV \qquad (3.16)$$

and the perturbation can be identified as

$$H_\delta = -\int h(\mathbf{r}(t))\frac{\delta T(\mathbf{r})}{T} dV \ . \qquad (3.17)$$

Then, we can write

$$\begin{aligned}\frac{\partial f_\delta^{(N)}}{\partial t} &= \{H_o, f_\delta^{(N)}\} + \{H_\delta, f_o^{(N)}\} \\ &= -i\Gamma_o f_\delta^{(N)} + \frac{f_o^{(N)}}{k_B T}\dot{H}_\delta \\ &= -i\Gamma_o f_\delta^{(N)} + \frac{f_o^{(N)}}{k_B T^2}\int h(\mathbf{r}(t))\delta T(\mathbf{r})dV \ . \end{aligned} \tag{3.18}$$

Then, applying energy conservation to express $h(\mathbf{r}(t))$ as $-\nabla\cdot\mathbf{j}$ and recognizing that heat flux on system boundaries is zero, we get

$$\begin{aligned}\frac{\partial f_\delta^{(N)}}{\partial t} &= -i\Gamma_o f_\delta^{(N)} + \frac{f_o^{(N)}}{k_B T^2}\int (-\nabla\cdot\mathbf{j})\,\delta T(\mathbf{r})dV \\ &= -i\Gamma_o f_\delta^{(N)} + \frac{f_o^{(N)}}{k_B T^2}\int \left[-\nabla\cdot(\mathbf{j}\delta T) + \mathbf{j}\cdot\nabla\delta T(\mathbf{r})\right]dV \\ &= -i\Gamma_o f_\delta^{(N)} + \frac{f_o^{(N)}}{k_B T^2}\nabla\delta T(\mathbf{r})\cdot\int \mathbf{j}dV \\ &= -i\Gamma_o f_\delta^{(N)} + \frac{V f_o^{(N)}}{k_B T^2}\nabla\delta T(\mathbf{r})\cdot\mathbf{J} \end{aligned} \tag{3.19}$$

where $\Gamma_o \equiv i\{H_o, \ \ \}$. The solution for $f_\delta^{(N)}$ is

$$f_\delta^{(N)}(t,\mathbf{r},\mathbf{p}) = -\frac{V}{k_B T^2}\nabla\delta T(\mathbf{r})\cdot\int_{-\infty}^{t} e^{-i(t-t_\delta)\Gamma_o}\mathbf{J}dt_\delta \ .$$

Then, the ensemble average of the system total heat flux per unit volume is

$$\begin{aligned}\langle J_x(t)\rangle &= \int\int J_x(\mathbf{r}(t),\mathbf{p}(t))\, f^{(N)}(t,(r),\mathbf{p})d\mathbf{r}d\mathbf{p} \\ &= -\frac{V}{k_B T^2}\int_{-\infty}^{t} dt_\delta \int\int J_x(\mathbf{r}(t),\mathbf{p}(t))\left[\nabla\delta T\cdot\mathbf{J}(\mathbf{r}(t_\delta),\mathbf{p}(t_\delta))\right] e^{-i(t-t_\delta)\Gamma_o}d\mathbf{r}d\mathbf{p} \\ &= -\frac{V}{k_B T^2}\int_{-\infty}^{t}\langle J_x(t)\mathbf{J}(t-t_\delta)\rangle\cdot\nabla\delta T \ . \end{aligned} \tag{3.20}$$

Then, we see that

$$k_{ij}(\omega) = \frac{V}{k_B T^2} \int_0^\infty \langle J_j(0) J_j(\tau) \rangle e^{-i\omega\tau} d\tau \ . \tag{3.21}$$

For an isotropic medium, we take an average of the thermal conductivity in the x, y, z directions:

$$k(\omega) = \frac{V}{3k_B T^2} \int_0^\infty \langle \mathbf{J}(0) \cdot \mathbf{J}(\tau) \rangle e^{-i\omega\tau} d\tau \ . \tag{3.22}$$

Equation 3.22 gives the thermal conductivity as a function of the perturbation frequency ω. For the bulk thermal conductivity, the perturbation frequency goes to 0 (i.e. constant heat fluxes) [72] so the appropriate expression for macroscopic thermal conductivity is

$$\kappa = \frac{V}{3k_B T^2} \int_0^\infty \langle \mathbf{J}(0) \cdot \mathbf{J}(\tau) \rangle d\tau \ . \tag{3.23}$$

3.3 Splitting Thermal Conductivity

The thermal conductivity in equation (3.23) is for a bulk system. Determining the contribution of each type of atomic interaction requires separating the heat flux carried by each type of interaction. The GROMOS potential treats the different types of atomic interactions separately, so using the definition for heat flux in equation (3.3), the contribution to the total heat flux of each type of interaction can be separated by first separating the stress due to that interaction. The total heat flux can be expressed as a sum of the heat flux due to each type of interaction:

$$\mathbf{S} = \mathbf{S_p} + \mathbf{S_b} + \mathbf{S_a} + \mathbf{S_d} \tag{3.24}$$

where the subscripts **p**, **b**, **a**, and **d** refer to pairs, bond stretching, angle bending, and dihedral interactions, respectively. Writing the stress in this way is the first step to teasing out the contributions to total heat transfer of each type of interactions and is along the same vein as [40]. Using equation (3.24) in equation (3.3), the heat flux can be written as

$$\mathbf{J} = \frac{1}{V}\sum_{i}^{N}\left(K_i\mathbf{v_i}\right) + \frac{1}{V}\sum_{i}^{N}\left(\phi_i\mathbf{v_i}\right) - \sum_{i}^{N}\left[\left(\mathbf{S_{pi}} + \mathbf{S_{bi}} + \mathbf{S_{ai}} + \mathbf{S_{di}}\right)\mathbf{v_i}\right] \tag{3.25}$$

where ϕ_i is the potential energy of the ith atom and can also be split into the component associated with each interaction. This fully breaks up the heat flux, except for the contributions from velocity, namely the kinetic energy K and the velocity of each atom. Using some algebraic manipulations,

$$\begin{aligned}
\mathbf{J} =& \frac{1}{V}\sum_{i}^{N}\left(K_i\mathbf{v_i}\right) + \frac{1}{V}\sum_{i}^{N}\left[\left(\phi_{pi} + \phi_{bi} + \phi_{ai} + \phi_{di}\right)\mathbf{v_i}\right] - \sum_{i}^{N}\left[\left(\mathbf{S_{pi}} + \mathbf{S_{bi}} + \mathbf{S_{ai}} + \mathbf{S_{di}}\right)\mathbf{v_i}\right] \\
=& \frac{1}{V}\sum_{i}^{N}\left(K_i\mathbf{v_i}\right) + \sum_{i}^{N}\left[\frac{1}{V}\left(\phi_{p_i} + \phi_{b_i} + \phi_{a_i} + \phi_{d_i}\right)\mathbf{v_i} - \left(\mathbf{S_{pi}} + \mathbf{S_{bi}} + \mathbf{S_{ai}} + \mathbf{S_{di}}\right)\mathbf{v_i}\right] \\
=& \frac{1}{V}\sum_{i}^{N}\left(K_i\mathbf{v_i}\right) + \sum_{i}^{N}\left[\left(\frac{\phi_{p_i}}{V} - \mathbf{S_{pi}} + \frac{\phi_{b_i}}{V} - \mathbf{S_{bi}} - \frac{\phi_{a_i}}{V} - \mathbf{S_{ai}} + \frac{\phi_{d_i}}{V} + \mathbf{S_{di}}\right)\mathbf{v_i}\right] \\
=& \frac{1}{V}\sum_{i}^{N}\left(K_i\mathbf{v_i}\right) + \sum_{i}^{N}\left(\frac{\phi_{p_i}}{V} - \mathbf{S_{pi}}\right)\mathbf{v_i} + \sum_{i}^{N}\left(\frac{\phi_{b_i}}{V} - \mathbf{S_{bi}}\right)\mathbf{v_i} + \sum_{i}^{N}\left(\frac{\phi_{a_i}}{V} - \mathbf{S_{ai}}\right)\mathbf{v_i} \\
&+ \sum_{i}^{N}\left(\frac{\phi_{d_i}}{V} - \mathbf{S_{di}}\right)\mathbf{v_i} \ .
\end{aligned} \tag{3.26}$$

From equation (3.26), define

$$\begin{aligned}
\mathbf{J_k} &= \frac{1}{V}\sum_i^N (K_i \mathbf{v_i}) \\
\mathbf{J_p} &= \sum_i^N \left(\frac{\phi_{p_i}}{V} - \mathbf{S_{pi}}\right)\mathbf{v_i} \\
\mathbf{J_b} &= \sum_i^N \left(\frac{\phi_{b_i}}{V} - \mathbf{S_{bi}}\right)\mathbf{v_i} \\
\mathbf{J_a} &= \sum_i^N \left(\frac{\phi_{a_i}}{V} - \mathbf{S_{ai}}\right)\mathbf{v_i} \\
\mathbf{J_d} &= \sum_i^N \left(\frac{\phi_{d_i}}{V} - \mathbf{S_{di}}\right)\mathbf{v_i}
\end{aligned} \tag{3.27}$$

Of course, the definitions enforce

$$\mathbf{J} = \mathbf{J_k} + \mathbf{J_p} + \mathbf{J_b} + \mathbf{J_a} + \mathbf{J_d} \tag{3.28}$$

as required. Using the definitions in equation (3.27), the flux autocorrelation can be broken into components.

$$\begin{aligned}
&\langle \mathbf{J}(0) \cdot \mathbf{J}(t) \rangle \\
&= \langle [\mathbf{J_k}(\mathbf{0}) + \mathbf{J_p}(0) + \mathbf{J_b}(0) + \mathbf{J_a}(0) + \mathbf{J_d}(0)] \cdot [\mathbf{J_k}(t) + \mathbf{J_p}(t) + \mathbf{J_b}(t) + \mathbf{J_a}(t) + \mathbf{J_d}(t)] \rangle
\end{aligned} \tag{3.29}$$

Applying the distributive property of dot products reveals

$$\begin{aligned}
&\langle \mathbf{J}(0)\cdot\mathbf{J}(t)\rangle = \\
&\quad \langle \mathbf{J_k}(0)\cdot\mathbf{J_k}(t)\rangle + \langle \mathbf{J_k}(0)\cdot\mathbf{J_p}(t)\rangle + \langle \mathbf{J_k}(0)\cdot\mathbf{J_b}(t)\rangle + \langle \mathbf{J_k}(0)\cdot\mathbf{J_a}(t)\rangle + \langle \mathbf{J_k}(0)\cdot\mathbf{J_d}(t)\rangle \\
&+ \langle \mathbf{J_p}(0)\cdot\mathbf{J_k}(t)\rangle + \langle \mathbf{J_p}(0)\cdot\mathbf{J_p}(t)\rangle + \langle \mathbf{J_p}(0)\cdot\mathbf{J_b}(t)\rangle + \langle \mathbf{J_p}(0)\cdot\mathbf{J_a}(t)\rangle + \langle \mathbf{J_p}(0)\cdot\mathbf{J_d}(t)\rangle \\
&+ \langle \mathbf{J_b}(0)\cdot\mathbf{J_k}(t)\rangle + \langle \mathbf{J_b}(0)\cdot\mathbf{J_p}(t)\rangle + \langle \mathbf{J_b}(0)\cdot\mathbf{J_b}(t)\rangle + \langle \mathbf{J_b}(0)\cdot\mathbf{J_a}(t)\rangle + \langle \mathbf{J_b}(0)\cdot\mathbf{J_d}(t)\rangle \\
&+ \langle \mathbf{J_a}(0)\cdot\mathbf{J_k}(t)\rangle + \langle \mathbf{J_a}(0)\cdot\mathbf{J_p}(t)\rangle + \langle \mathbf{J_a}(0)\cdot\mathbf{J_b}(t)\rangle + \langle \mathbf{J_a}(0)\cdot\mathbf{J_a}(t)\rangle + \langle \mathbf{J_a}(0)\cdot\mathbf{J_d}(t)\rangle \\
&+ \langle \mathbf{J_d}(0)\cdot\mathbf{J_k}(t)\rangle + \langle \mathbf{J_d}(0)\cdot\mathbf{J_p}(t)\rangle + \langle \mathbf{J_d}(0)\cdot\mathbf{J_b}(t)\rangle + \langle \mathbf{J_d}(0)\cdot\mathbf{J_a}(t)\rangle + \langle \mathbf{J_d}(0)\cdot\mathbf{J_d}(t)\rangle
\end{aligned} \tag{3.30}$$

The effective thermal conductivity is for heat conduction between any two types of interactions is

$$\kappa_{ij} = \frac{V}{3k_B T^2}\int_0^\infty \langle \mathbf{J}_i(0)\cdot\mathbf{J}_j(t)\rangle dt \tag{3.31}$$

where the subscripts i and j refers to the two types of interactions. Thus, calculating an effective "thermal conductivity" for interaction type i requires the dot product of the flux due i. Cross correlations $\mathbf{J}_i(0)\cdot\mathbf{J}_j(t)$ represent the transfer of energy from interaction type i to interaction type j and is a major component of heat transfer in octane. Indeed, these cross correlations are what makes heat transfer in bulk molecular chain liquids possible since, as established previously, heat transfer pathways in these systems must pass through multiple types of interactions.

Chapter 4

Calculation Procedures

The previous chapters introduced the methods of obtaining accurate molecular trajectories and the necessary theory to analyze the trajectory to obtain thermal transfer properties. This chapter covers the specifics about applying the topics discussed previously to bulk octane and includes the necessary simulation system parameters.

4.1 System Convergence

As discussed previously, the time step must balance between minimizing errors from integration and computational efficiency. Typically, the time step is set by the need to keep the system energy stable. Additionally, the time step must be small enough so the atoms in the system do not move too far in each step and crash into each other. To converge the energy in the simulated system, a time step of 1 fs is required (figure 4-1a). However, the heat flux correlations show oscillations with a period of about 6 fs so a smaller time step of 0.1 fs was chosen to produce a smooth heat flux curve.

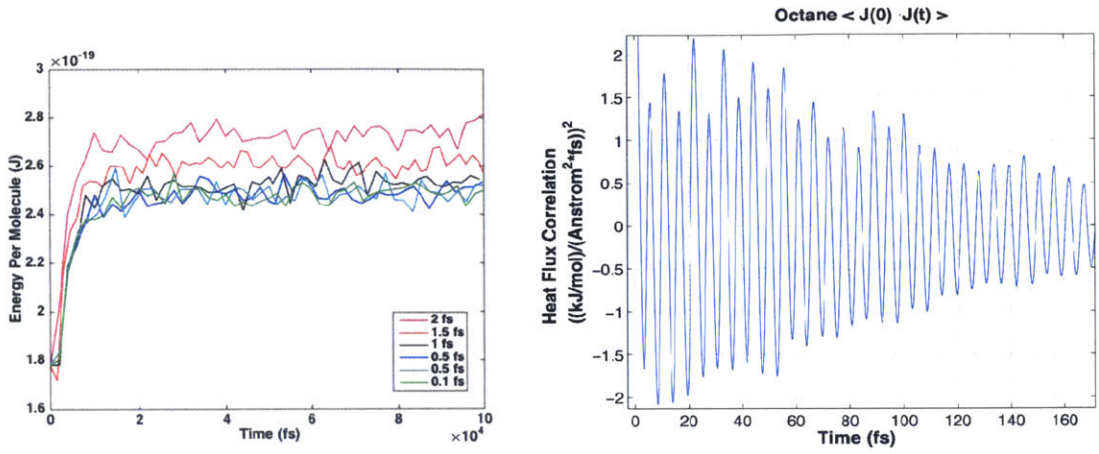

(a) (b)

Figure 4-1: The time step size was found in two steps. (a) The first limit on time step size is the convergence of energies. The fluctuations over time in total energy per octane molecule is plotted for several time step sizes. As the time step becomes bigger than 1 fs, the energy becomes inaccurate. Convergence in energy is reached at 1 fs, and smaller time steps do not significantly alter the energy. (b) The heat flux correlation (the beginning of on example) is shown here, has oscillations around 170 THz, which a time step size of 1 fs cannot accurately capture. Therefore, the time step size of 0.11 fs was chosen to produce smooth correlations.

As discussed in chapter 2, the size of the base cell often affects computed properties. The base cell used in this thesis contains 1125 octane molecules, which was chosen to balance between computational speed and accuracy of the computed thermal conductivity (figure 4-2). Increasing the base cell to 1944 octane molecules changes the calculated thermal conductivity by less than 10% but almost doubles the total computational time needed. The base cell is a 67 Å × 67 Å × 67 Å cube, and periodic boundary conditions are used during calculations.

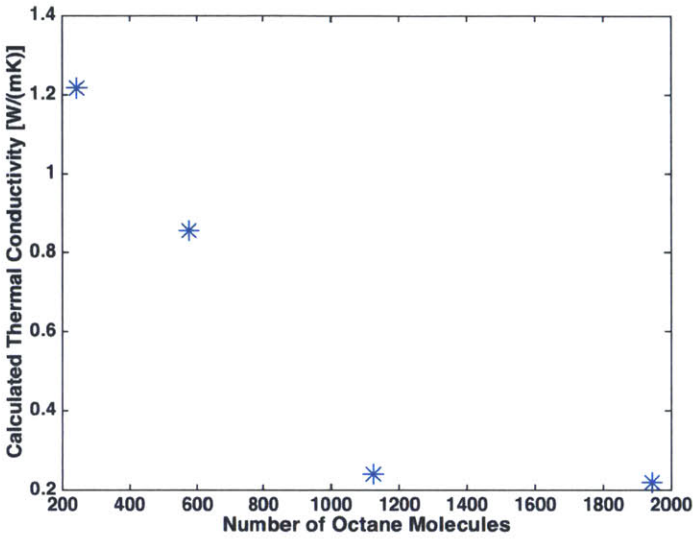

Figure 4-2: The system size must be large enough to converge the calculated thermal conductivity. Acceptable convergence is reached at a system containing 1125 octane molecules. Increasing the system to 1944 octane molecules changes the calculated thermal conductivity by less than 10%. Each thermal conductivity value in the plot is the average of 6 separate runs.

4.2 Choosing Equilibration Time

The initial system is created using a regular arrangement of octane molecules matched to the experimental density, as shown in figure 4-3. Equilibration then serves the dual purpose of randomizing the molecule positions and distributing the kinetic and potential energies to give stable system temperatures and pressures even after the thermostats and barostat have been removed. The cartesian coordinates of each atom before and after a 10 ps equilibration is plotted in figure 4-4. No discernible patterns remain, showing that the equilibration time is sufficient to randomize the position of the molecules.

The equilibration is broken into two phases, as shown in figure 4-5, each lasting 5 ps in simulated time. The first phase is in NVT while the second is NVE. System energy

and temperature stabilizes after about 2 ps of NVT equilibration. Even after the thermostat is removed, the system temperature remains stable during the subsequent NVE equilibration, indicating that the system energy has been distributed appropriately between kinetic and potential energy during the NVT equilibration phase. The constant temperature in NVE ensembles allows the NVE ensemble to be used for collecting data for the Green-Kubo formula for thermal conductivity and ensures that the Green-Kubo formula applies to this system. The first 2 ps of the production run after the two equilibration phases are also shown in figure 4-5. The production run is in NVE and also shows stable system temperatures.

The production run lasts for a total of 10 ps. An example of the heat flux correlation calculated during the production run is shown in figure 4-6. Note that the correlation decays to small oscillations around zero after about 1.5 ps in simulated time. The calculated thermal conductivity also begins to oscillate around the final value of 0.24 W/(mK) after about 1.5 ps (figure 4-7).

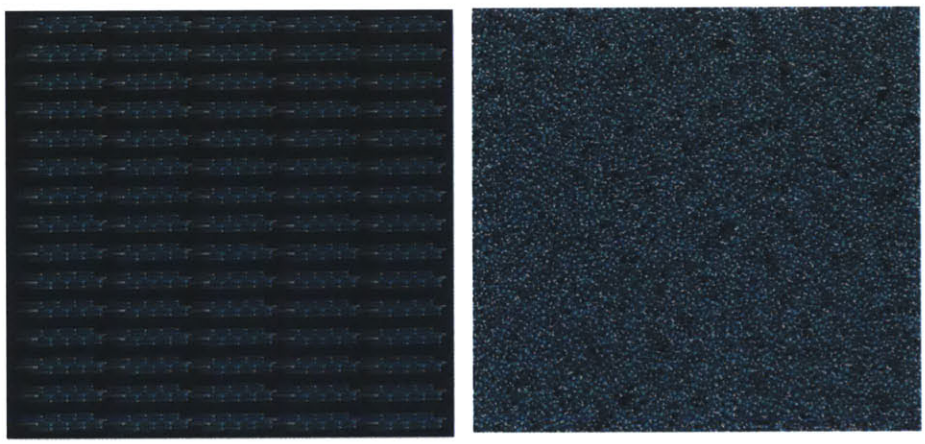

(a) (b)

Figure 4-3: Images of the simulation system projected onto the x-y plane. The system consists of a 67 Å $\times$ 67 Å $\times$ 67 Å cubic base cell containing 1125 octane molecules and periodic boundary conditions. (a) The initial system is created by arranging octane molecules in a regular pattern. (b) The system after equilibration has randomized the atomic positions.

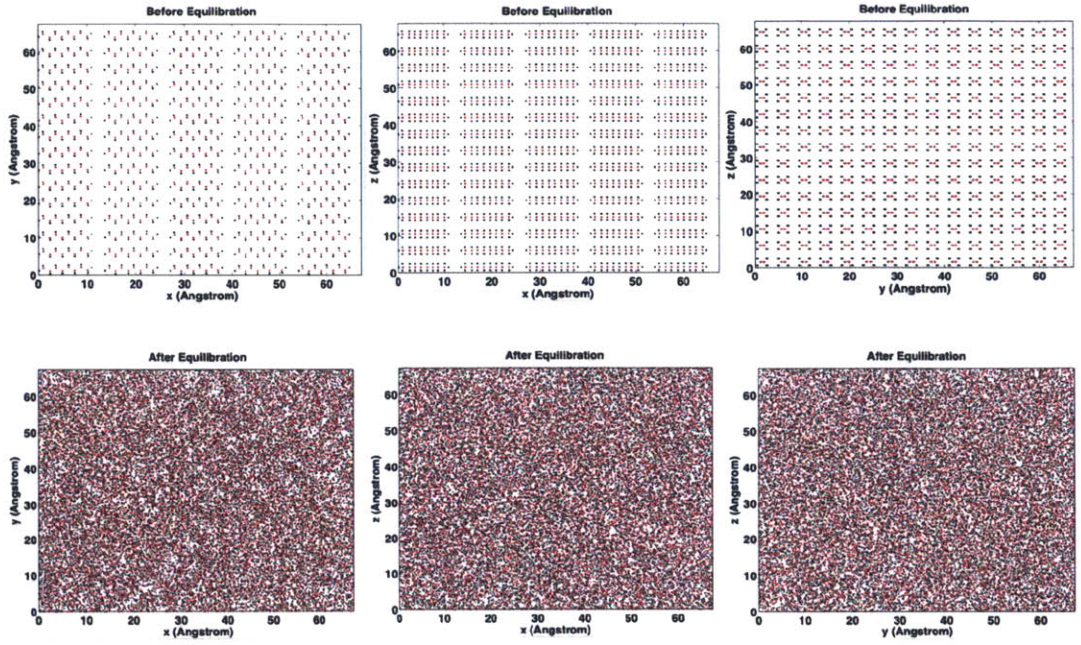

Figure 4-4: Plots of atomic positions along the x, y, and z axis showing the positions of each hydrogen (black) and carbon (red) atom before and after equilibration. No orderly pattern remains after equilibration, showing the system is fully randomized.

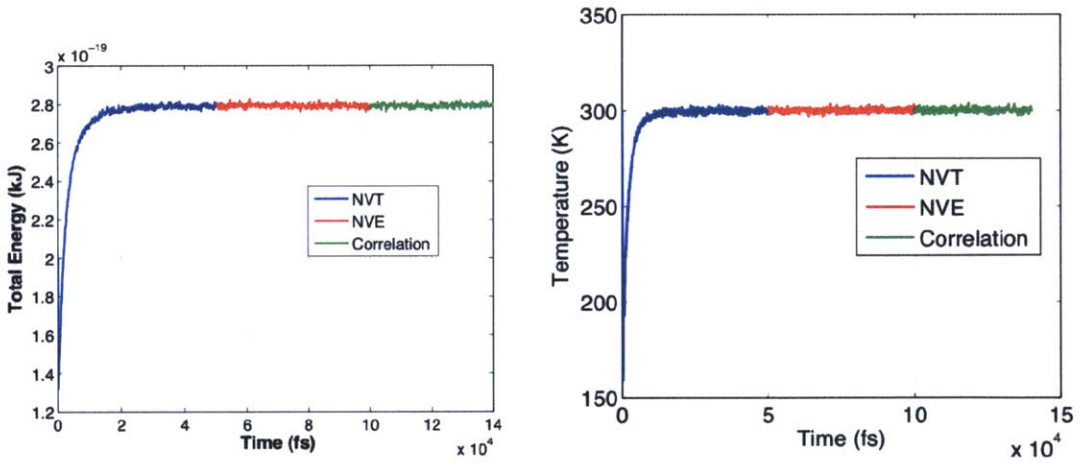

(a) (b)

Figure 4-5: Plot of the system energy and temperature during NVT and NVE equilibration and during the beginning of the production run.

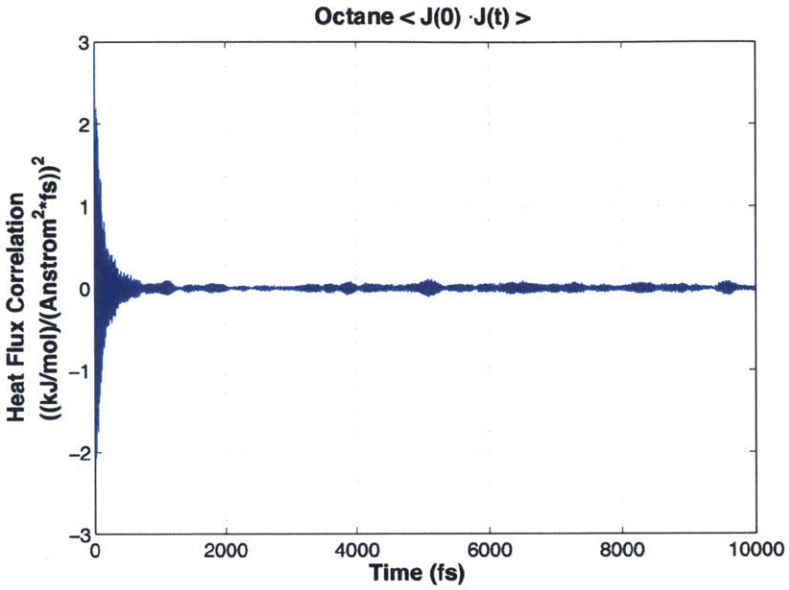

Figure 4-6: An example of the calculated correlation function for the octane system. The correlations decay to small oscillations around zero after about 1.5 ps.

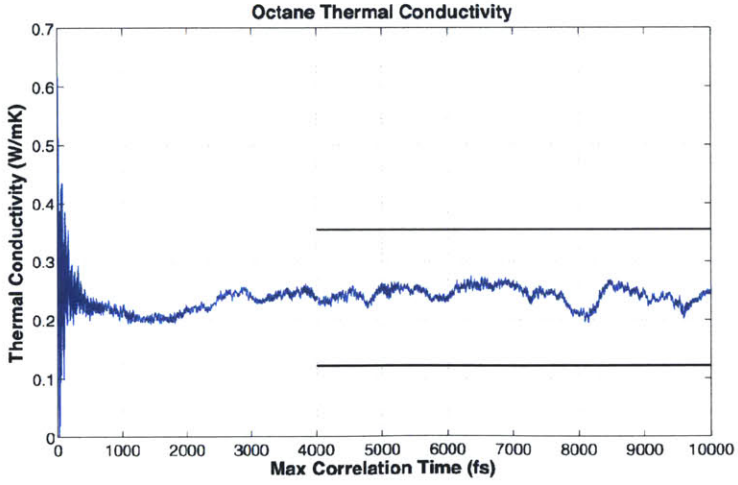

Figure 4-7: Calculated thermal conductivity as a function of the maximum correlation time in the integral. This is the average of 10 separate simulation runs. The average value is 0.24 W/(mK). Black bars denote the boundaries of the expected error.

Chapter 5

Results and Discussion

This chapter covers the results from the simulations and discusses the significance of the results to shed more insight into heat transfer in bulk octane.

5.1 Comparison to Experimental Data

As a numerical method, results from molecular dynamics simulations of a system should be validated against experimental results. The density presents a simple check. The density for a range of temperatures for the octane system is shown in figure 5-1. The calculated values reproduce the experimental trend and the difference between the calculated value and the experimental ones is less than 10%. A second check is to compare the calculated overall thermal conductivity against experimental values. The calculated total thermal conductivity of the system, which is the average of 10 separate runs, is shown in figure 4-7. The average value is 0.24±0.11 W/(mK). The experimentally measured thermal conductivity for octane is around 0.13 W/(mK) [73], which is within the expected error. The comparisons with experimental values show that the simulated system does capture the behavior of bulk octane and validates the

simulation parameters.

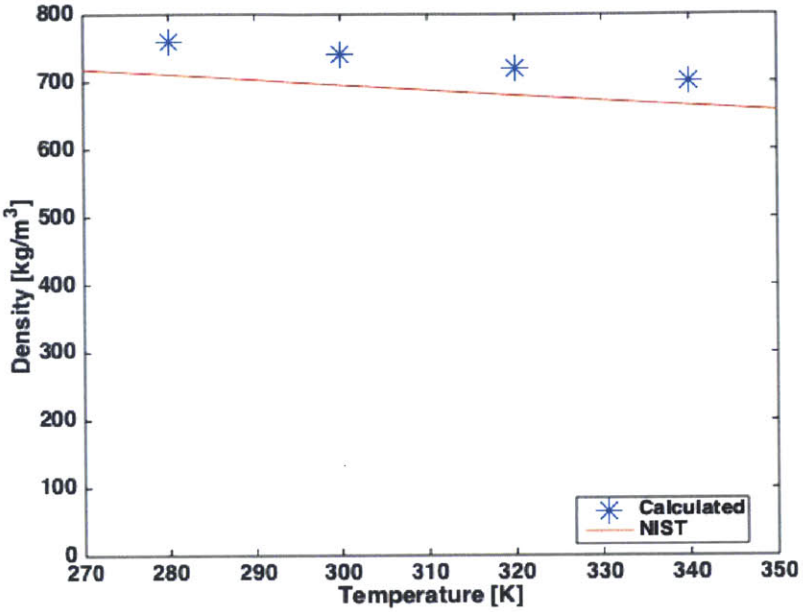

Figure 5-1: Density of the calculated octane MD system and experimental results from NIST [73]. The calculated values reproduce the trend from experimental vales. The error between calculated and experimental values is about 10%.

5.2 Effective Thermal Conductivities

The total thermal conductivity was split into the contribution from each type of interaction using the methods previously described in chapter 3 and shown in figure 5-2. All the results from this section are the averages from 10 separate simulation runs where the only difference is the random number seed. These effective thermal conductivities are calculated using the heat flux over all the atoms in the system and so are averages over the entire system. Of the effective thermal conductivities, the ones that involve pairs, bond stretching, angles bending, and kinetic energy terms are significant while the ones that involve dihedral interactions are all essentially zero.

This means that dihedral interactions carry negligible amounts of heat through the bulk octane system. The effective thermal conductivity of bond stretching (bb) is the highest, meaning that most heat in the system is transferred by bond stretching exciting other bond stretching modes. This is in line with the fact that carbon-carbon bonds are every effective at conducting heat [1]. Pair-pair interactions (as described in chapter 2, the pairs interactions are the sum of the van der Waals and electrostatic interactions), are almost as high as bond-bond interactions. On the surface, this is a bit surprising since van der Waals and electrostatic interactions in alkanes are much weaker than bond interactions. However, the pair-pair interaction is a major part of intermolecular heat transfer and previous non-equilibrium MD results have shown that intermolecular interactions account for about 50% of total heat transfer in bulk octane [27]. Therefore, it is reasonable for pair-pair interactions to have a fairly high effective thermal conductivity in comparison to the other interactions.

The effective thermal conductivities can be split into two categories: intermolecular heat transfer and intramolecular heat transfer. Specifically, effective thermal conductivities involving only bonds, angles, and dihedrals are intramolecular heat transfer since these interactions are limited to atoms within the same molecule. Intermolecular heat transfer requires at least one of the interactions to be pairs or kinetic energy since these are the interactions that can carry heat from one molecule to another. The sums of the two categories are 0.14 W/(mK) for intramolecular heat transfer and 0.10 W/(mK) for intermolecular heat transfer. This can be understood in the context of a circuit analogy for heat transfer, as shown in figure 5-3. In the analogy, the thermal resistance for heat transfer along the chain and between the chain are in series so no matter how large the intramolecular heat transfer is, the thermal conductivity in the bulk system will not be significantly increased unless intermolecular heat transfer is also high. The result that the thermal conductivity within a molecule is only 0.14 W/(mK) is surprising since previous studies have shown that the carbon-carbon bond is capable of high heat transfer, but the thermal conductiv-

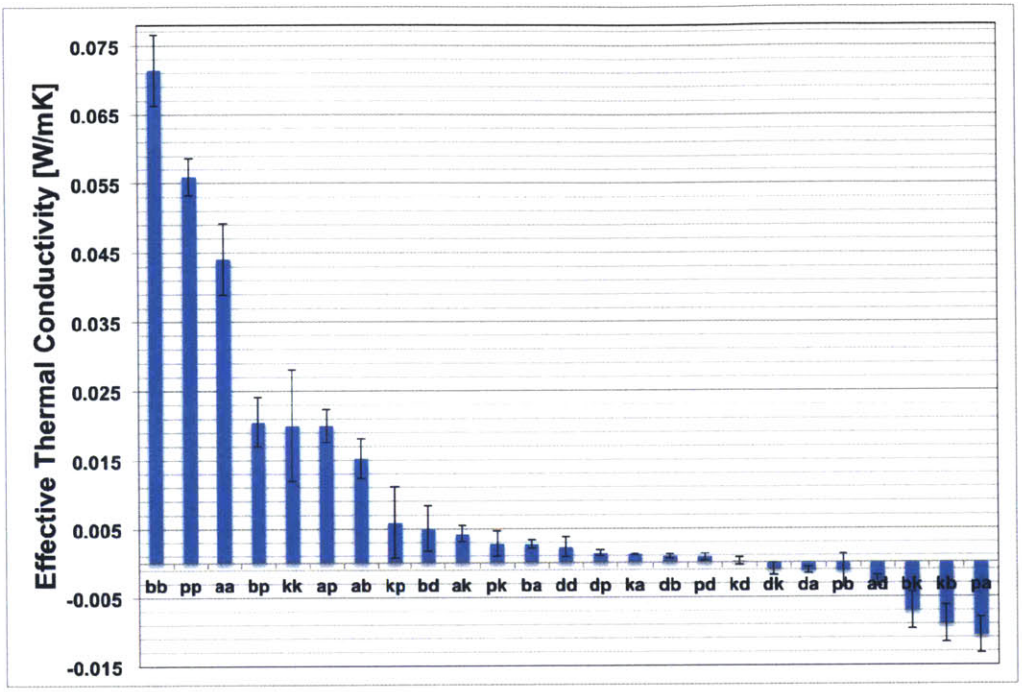

Figure 5-2: The total thermal conductivity has been split into effective thermal conductivities for each type of interaction. Pairs, bond stretching, angle bending, dihedral, and kinetic energy terms are labeled by p, b, a, d, and k, respectively. The first letter denotes the interaction providing $\mathbf{J}(0)$ in the correlation $\langle \mathbf{J}(0) \cdot \mathbf{J}(t) \rangle$, and the second letter denotes the interaction providing $\mathbf{J}(t)$. The effective thermal conductivities include correlations of an interaction with itself (the two letters in the label are the same) and cross interactions between different types of interactions (the two letters in the label are different).

ity of a single carbon chain becomes smaller as the length decreases [1] since, as the chains get shorter, longer wavelength phonon modes are eliminated and the length of the chain limits mean free path, which both significantly reduce thermal conductivity. Additionally, in a bulk system, the heat transfer within a molecule is further disrupted by interactions with surrounding molecules.

In figure 5-2, several interactions produce negative terms. On the surface, this seems to indicate heat flowing from a colder area to a hotter area, which would be a violation of the Second Law of Thermodynamics. However, these interactions cannot occur without the other interactions so the net thermal conductivity is still positive and

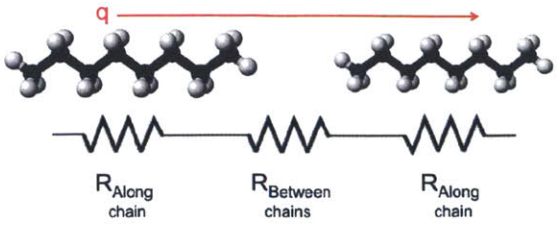

Figure 5-3: Circuit analogy for heat transfer in bulk octane. Because intermolecular and intramolecular heat transfer are in series, only increasing one will not be enough to drastically increase bulk thermal conductivity.

does not violate the Second Law. These negative terms can be understood as heat flux exchanges and this situation would be similar to radiative heat exchange, where the radiation from the colder body to the hot body must also be accounted for to arrive at the correct net heat transfer. Negative thermal conductivity was also observed in MD studies on single polyethylene molecules [72]. Additionally, non-equilibrium MD studies on water have also observed heat flux in the opposite direction of the temperature gradient [29].

Chapter 6

Conclusion

6.1 Summary

Understanding heat transfer in liquids at the atomic level would greatly enhance the arsenal of tools for thermal engineering by allowing liquids with specific properties to be designed. This thesis uses equilibrium MD and the Green-Kubo formula to model the heat transfer in bulk octane and introduces a method of splitting the total thermal conductivity into the effective thermal conductivity due to each type of atomic interactions. The effective thermal conductivities were calculated for bulk octane. When taken over the entire system, intramolecular and intermolecular heat transfer in bulk octane are both significant components of the total heat transfer, with the intramolecular effective thermal conductivity being 0.14 W/(mK) and intermolecular effective thermal conductivity being 0.1 W/(mK). Heat transfer in the carbon backbone of bulk octane is not nearly as high as that in the carbon backbone of polyethylene [1].

6.2 Future Work

This thesis has explored thermal transport in bulk octane with equilibrium MD, but many questions of atomic level thermal transfer remains unanswered. Calculations at different temperatures and pressures could further link atomic interactions to thermal conductivity and analysis of the the molecular conformation could identify shapes that are more effective heat carriers. There are also additional types of interactions, like hydrogen bonding, to be explored.

Octane is a simple chain molecule and do not contain features found in more complex molecules, such as functional groups. The addition of other elements would likely significantly complicate the heat transfer picture. On one hand, functional groups can introduce stronger intermolecular interactions into the system that would boost intermolecular heat transfer. On the other hand, functional groups could disrupt heat transfer along the chain backbone and decrease intramolecular heat transfer. A detailed analysis would be required to fully explore how these two factors balance in the bulk heat transfer of the system.

Bibliography

[1] A. Henry and G. Chen. High thermal conductivity of single polyethylene chains using molecular dynamics simulations. *Physical Review Letters*, 101:235502, 2008.

[2] A. J. H. McGaughey and M. Kaviany. Phonon transport in molecular dynamics simulations: Formulation and thermal conductivity prediction. *Advances in Heat Transfer*, 39:169–255, 2006.

[3] M. H. Ernest, L. K. Haines, and J. R. Dorfman. Theory of transport coefficients for moderately dense gases. *Reviews of Modern Physics*, 41:296–316, 1969.

[4] O. Guvench and A. D. MacKerell, Jr. *Molecular Modeling of Proteins.* Humana Press, Totowa, NJ, 2008.

[5] Thomson Reuters. Web of Science <apps.webofknowledge.com>.

[6] S. J. Plimpton. Fast parallel algorithms for short-range molecular dynamics. *Journal of Computational Physics*, 117:1–19, 1995.

[7] Sandia National Laboratories. LAMMPS <http://lammps.sandia.gov>.

[8] W. Lee, K. Kim, W. Jeong, L. A. Zotti, F. Pauly, J. C. Cuevas, and P. Reddy. Heat dissipation in atomic-scale junctions. *Nature*, 498:209–212, 2013.

[9] J. Huang, J. Park, W. Wang, C. J. Murphy, and D. G. Cahill. Ultrafast thermal analysis of surface functionalized gold nanorods in aqueous solution. *ACS Nano*, 7:589–597, 2013.

[10] Z. Huang, F. Chen, R. D'agosta, P. A. Bennett, M. D. Ventra, and N. Tao. Local ionic and electron heating in single-molecule junctions. *Nature Nanotechnology*, 2:698–703, 2007.

[11] N. Li, J. Ren, L. Wang, G. Zhang, P. Hanggi, and B. Li. Phononics: Manipulating heat flow with electronic analogs and beyond. *Review of Modern Physics*, 84:1045–1066, 2012.

[12] D. R. Ward, D. A. Corley, J. M. Tour, and D. Natelson. Vibrational and electronic heating in nanoscale junctions. *Nature Nanotechnology*, 6:33–38, 2011.

[13] A. E. Nasrabad, R. Laghaei, and B. C. Eu. Molecular theory of thermal conductivity of the Lennard-Jones fluid. *Journal of Chemical Physics*, 124:084506, 2006.

[14] R. Vogelsang, C. Hoheisel, and G. Ciccotti. Thermal conductivity of the Lennard-Jones liquid by molecular dynamics calculations. *Journal of Chemical Physics*, 86:6371–6375, 1987.

[15] J. E. Jones. On the determination of molecular fields. II. From the equation of state of a gas. *Proceedings of the Royal Society of London series A*, 106:463–477, 1924.

[16] M. Bugel and G. Galliero. Thermal conductivity of the Lennard-Jones fluid: An empirical correlation. *Chemical Physics*, 352:249–257, 2008.

[17] K. V. Tretiakov and S. Scandolo. Thermal conductivity of solid argon from molecular dynamics simulations. *Journal of Chemical Physics*, 120:3765–3769, 2004.

[18] R. Vogelsang, C. Hoheisel, G. V. Paolini, and G. Ciccotti. Soret coefficient of isotopic Lennard-Jones mixtures and the Ar-Kr system as determined by equilibrium molecular-dynamics calculations. *Physical Review A*, 36:3964–3974, 1987.

[19] J. M. Haile. *Molecular Dynamics Simulation: Elementary Methods.* Wiley-Interscience, 1997.

[20] T. Ikeshoji and B. Hafskjold. Non-equilibrium molecular dynamics calculation of heat conduction in liquid and through liquid-gas interface. *Molecular Physics*, 81:251–261, 1993.

[21] F. Muller-Plathe. A simple nonequilibrium molecular dynamics method for calculating the thermal conductivity. *Journal of Chemical Physics*, 106:6082–6085, 1997.

[22] F. C. Collins and H. Raffel. Statistical mechanical theory of transport processes in liquids. *Free-Conventional Heat Transfer*, 29:699–710, 1958.

[23] R. W. Zwangzig, J. G. Kirkwood, I. Oppenheim, and B. J. Alder. Statistical mechanical theory of transport processes. VI. The coefficient of thermal conductivity of monatomic liquids. *Journal of Chemical Physics*, 22:783–790, 1954.

[24] M. S. Green. Markoff random processes and the statistical mechanics of time-dependent phenomena. II. Irreversible processes in fluids. *Journal of Chemical Physics*, 22:398–413, 1954.

[25] R. Kubo. Statistical-mechanical theory of irreversible processes. I. General theory and simple applications to magnetic and conduction problems. *Journal of the Physical Society of Japan*, 12:570–586, 1957.

[26] A. Uhlir Jr. Thermal conductivity of fluid argon and nitrogen. *Journal of Chemical Physics*, 20:463–472, 1952.

[27] T. Ohara, T. C. Yuan, D. Torii, G. Kikugawa, and N. Kosugi. Heat conduction in chain polymer liquids: Molecular dynamics study on the contributions of inter- and intramolecular energy transfer. *Journal of Chemical Physics*, 135:034507, 2011.

[28] G. V. Paolini, G. Ciccotti, and C. Massobrio. Nonlinear thermal response of a Lennard-Jones fluid near the triple point. *Physical Review A*, 34:1355–1362, 1986.

[29] T. Ohara. Intermolecular energy transfer in liquid water and its contribution to heat conduction: A molecular dynamics study. *Journal of Chemical Physics*, 111:6492–6500, 1999.

[30] K. Singer, A. Taylor, and J. V. L. Singer. Thermodynamic and structural properties of liquids modelled by '2-Lennard-Jones centres' pair potentials. *Molecular Physics*, 33:1757, 1977.

[31] T. Tokumasu, T. Ohara, and K. Kamijo. Effect of molecular elongation on the thermal conductivity of diatomic liquids. *Journal of Chemical Physics*, 118:3677–3685, 2003.

[32] T. Tokumasu and K. Kamijo. Molecular dynamics study for the thermal conductivity of diatomic liquid. *Superlattices and Microstructures*, 35:217–225, 2004.

[33] W. L. Jorgensen and J. Tirado-Rives. The OPLS [optimized potentials for liquid simulations] potential functions for proteins, energy minimizations for crystals of cyclic peptides and crambin. *Journal of the American Chemical Society*, 110:1657–1666, 1988.

[34] B. R. Brooks, C. L. Brooks III, A. D. Mackerell, L. Nilsson, R. J. Petrella, B. Roux, Y. Won, G. Archontis, C. Bartels, S. Boresch, A. Caflisch, L. Caves, Q. Cui, A. R. Dinner, M. Feig, S. Fischer, J. Gao, M. Hodoscek, W. Im, K. Kuczera, T. Lazaridis, J. Ma, V. Ovchinnikov, E. Paci, R. W. Pastor, C. B. Post, J. Z. Pu, M. Schaefer, B. Tidor, R. M. Venable, H. L. Woodcock, X. Wu, W. Yang, D. M. York, and M. Karplus. CHARMM: The biomolecular simulation program. *Journal of Computational Chemistry*, 30:1545–1614, 2009.

[35] D. Case, V. Babin, J. Berryman, R. Betz, Q. Cai, D. Cerutti, T. Cheatham, III, T. Darden, R. Duke, H. Gohlke, A. Goetz, S. Gusarov, N. Homeyer, P. Janowski, J. Kaus, I. Kolossváry, A. Kovalenko, T. Lee, S. LeGrand, T. Luchko, R. Luo, B. Madej, K. Merz, F. Paesani, D. Roe, A. Roitberg, C. Sagui, R. Salomon-Ferrer, G. Seabra, C. Simmerling, W. Smith, J. Swails, R. Walker, J. Wang, R. Wolf, X. Wu, and P. Kollman. AMBER 14. University of California, San Francisco, 2014.

[36] C. Oostenbrink, A. Villa, A. E. Mark, and W. F. V. Gunsteren. A biomolecular force field based on the free enthalpy of hydration and solvation: The GROMOS force-field parameter sets 53A5 and 53A6. *Journal of Computational Chemistry*, 25:1656–1676, 2004.

[37] D. Bedrov and G. D. Smith. Thermal conductivity of molecular fluids from molecular dynamics simulations: Application of a new imposed-flux method. *Journal of Chemical Physics*, 113:8080, 2000.

[38] D. K. Dysthe, A. H. Fuchs, and B. Rousseau. Fluid transport properties by equilibrium molecular dynamics. III. Evaluation of united atom interaction potential models for pure alkanes. *Journal of Chemical Physics*, 112:7581–7590, 2000.

[39] G. Guevara-Carrion, C. Nieto-Draghi, J. Vrabec, and H. Hasse. Prediction of transport properties by molecular simulation: Methanol and ethanol and their mixture. *Journal of Physical Chemistry B*, 112:16664–16674, 2008.

[40] Y.-S. Lin, P.-Y. Hsiao, and C.-C. Chieng. Constructing a force interaction model for thermal conductivity computation using molecular dyanmics simulation: Ethylene glycol as an example. *Journal of Chemical Physics*, 134:154509, 2011.

[41] J. Petravic. Thermal conductivity of ethanol. *Journal of Chemical Physics*, 123:174503, 2005.

[42] E. J. Rosenbaum, N. J. English, J. K. Johnson, D. W. Shaw, and R. P. Warzinski. Thermal conductivity of methane hydrate from experiment and molecular simulation. *Journal of Physical Chemistry B*, pages 13194–13205, 2007.

[43] M. Zhang, E. Lussetti, L. E. S. de Souza, and F. Muller-Plathe. Thermal conductivities of molecular liquids by reverse nonequilibrium molecular dynamics. *Journal of Physical Chemistry B*, 31:15060–15067, 2005.

[44] S. Shen, A. Henry, J. Tong, R. Zheng, and G. Chen. Polyethylene nanofibres with very high thermal conductivities. *Nature Nanotechnology*, 5:251–255, 2010.

[45] J. Liu and R. Yang. Tuning the thermal conductivity of polymers with mechanical strains. *Physical Review B*, 81:174122, 2010.

[46] A. V. Savin and O. I. Savina. Dependence of the thermal conductivity of a polymer chain on its tension. *Physics of the Solid State*, 56:1664–1672, 2014.

[47] T. Zhang and T. Luo. Morphology-influenced thermal conductivity of polyethylene single chains and crystalline fibers. *Journal of Applied Physics*, 112:094304, 2012.

[48] G.-J. Hu, B.-Y. Cao, and Y.-W. Li. Thermal conduction in a single polyethylene chain using molecular dynamics simulations. *Chinese Physics Letters*, 31:086501, 2014.

[49] J. Zhao, J.-W. Jiang, N. Wei, Y. Zhang, and T. Rabczuk. Thermal conductivity dependence on chain length in amorphous polymers. *Journal of Applied Physics*, 113:184304, 2013.

[50] J. Liu and R. Yang. Length-dependent thermal conductivity of single extended polymer chains. *Physical Review B*, 86:104307, 2012.

[51] T. Zhang, X. Wu, and T. Luo. Polymer nanofibers with outstanding thermal conductivity and thermal stability: Fundamental linkage between molecular characteristics and macroscopic thermal properties. *Journal of Physical Chemistry C*, 118:21148–21159, 2014.

[52] D. Torii, T. Nakano, and T. Ohara. Contribution of inter- and intramolecular energy transfers to heat conduction in liquids. *The Journal of Chemical Physics*, 128:044504, 2008.

[53] X. Li and H. Gao. Atomistic modelling of deformation and failure mechanisms in nanostructured materials. *National Science Review*, doi: 10.1093/nsr/nwu049, 2014.

[54] National Nanotechnology Initiative. What's so special about the nanoscale? <http://www.nano.gov/nanotech-101/special>, Jan. 20, 2015.

[55] R. E. Rudd and J. Q. Broughton. Coarse-grained molecular dynamics and the atomic limit of finite elements. *Physical Review B*, 58:R5893–R5896, 1998.

[56] C. Oostenbrink, T. A. Soares, N. F. A. van der Vegt, and W. F. van Gunsteren. Validation of the 53A6 GROMOS force field. *European Biophysics Journal*, 34:273–284, 2005.

[57] L. Cartz. Thermal vibrations of atoms in cubic crystals II: The amplitude of atomic vibrations. *Proceedings of the Physical Society. Section B*, 68:957–967, 1955.

[58] D. Frenkel and B. Smit. *Understanding Molecular Simulation: From Algorithms to Appliations.* Academic Press, 2001.

[59] R. A. Buckingham. The classical equation of state of gaseous helium, neon and argon. *Proceedings of the Royal Society of London. Series A*, 1938.

[60] L. Verlet. Computer "experiments" on classical fluids. I. Thermodynamical properties of Lennard-Jones molecules. *Physical Review*, 159:98–103, 1967.

[61] Folding at Home <http://folding.stanford.edu>.

[62] G. B. Arfken, H.-J. Weber, and F. E. Harris. *Mathematical Methods for Physicists.* Academic Press, 2012.

[63] M. R. Hestenes and E. Stiefel. Methods of conjugate gradients for solving linear systems. *Journal of Research of the National Bureau of Standards*, 49:409–436, 1952.

[64] P. Wriggers. *Nonlinear Finite Elements Methods.* Springer Science & Business Media, 2008.

[65] H. J. C. Berendsen, J. P. M. Postma, W. F. van Gunsteren, A. DiNola, and J. R. Haak. Molecular dynamics with coupling to an external bath. *Journal of Chemical Physics*, 81:3684–3690, 1984.

[66] Sandia National Laboratories. *LAMMPS Users Manual*, Feb 1, 2014 edition.

[67] W. G. Hoover. Canonical dynamics: Equilibrium phase-space distributions. *Physical Review A*, 31:1695–1697, 1985.

[68] S. Nose. A unified formulation of the constant temperature molecular-dynamics methods. *Journal of Chemical Physics*, 81:511–519, 1984.

[69] P. H. Hunenberger. *Advanced Computer Simulation: Approaches for Soft Matter Science*, volume 173 of *Advances in Polymer Science*, chapter Thermostat Al-

gorithms for Molecular Dynamics Simulations, pages 105–149. Springer Berlin Heidelberg, 2005.

[70] G. Chen. *Nanoscale Energy Transport and Conversion : A Parallel Treatment of Electrons, Molecules, Phonons, and Photons: A Parallel Treatment of Electrons, Molecules, Phonons, and Photons*, chapter 10. Molecular Dynamics Simulation. Oxford University Press, 2005.

[71] D. H. Tsai. The virial theorem and stress calculation in molecular dynamics. *Journal of Chemical Physics*, 70:1375–1382, 1979.

[72] A. S. F. Henry. *1D-to-3D Transition of Phonon Heat Conduction in Polyethlyene Using Molecular Dynamics Simulations.* PhD thesis, Massachusetts Institute of Technology, 2009.

[73] National Institute of Standards and Technology. NIST Chemistry WebBook <http://webbook.nist.gov/chemistry/>.